ATLAS NOTE

ATL-PHYS-PUB-2011-008

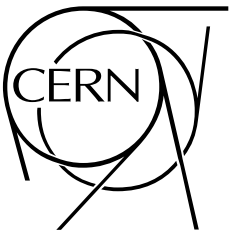

May 5, 2011

New ATLAS event generator tunes to 2010 data

The ATLAS collaboration

Abstract

This note describes new Monte Carlo event generator tunings for the Pythia 6 and Herwig/Jimmy generators, made making maximal use of the available published data from ATLAS as well as the Tevatron and LEP experiments. New considerations in this tuning include the improvement of the description of e^+e^- event shape and jet rate data, and on description of hadron collider event shape observables in Pythia, in addition to the established procedure of tuning the multiple parton interactions of both models to describe underlying event and minimum bias data. The tuning of Pythia uses the MRST LO** PDF, while the purely MPI tune of Herwig/Jimmy has been performed for ten different PDFs. Both models have difficulty describing all features of the available MPI-sensitive observables, resulting in separate minimum bias and underlying event tunes (AMBT2 and AUET2) for Pythia.

Contents

Introduction

Since the start-up of the LHC in 2009, ATLAS has collected 47 pb^{-1} of data at 7 TeV centre-of-mass energy. This entry into a new energy regime has provided, from the point of view of MC event generators, an opportunity to experimentally test extrapolated predictions of QCD from lower energies, and to improve that description for new physics studies at 7 TeV and beyond. ATLAS has measured many QCD observables at 900 GeV and 7 TeV, ranging from purely soft QCD in minimum bias events [1], though low-to-medium $p_\perp$ measurements of the evolution of underlying event observables [2, 3], and up to hard QCD processes such as jet distributions up to $p_\perp(\text{jet}) \sim 2$ TeV [4].

In this note, we summarise the effort within ATLAS to provide MC generator parameter sets – "tunes" which provide an optimal description of this ATLAS data for use in future LHC physics studies. These tunes have been constructed for the Pythia 6 and Herwig/Jimmy event generators, and intended for use as the main ATLAS configurations of these generators in the ATLAS 2011 MC simulation production campaign ("MC11"). Our tuning of Pythia 6 attempts to be comprehensive, starting with an optimisation of final state parameters based on e^+e^- collider data and then tuning both initial state radiation (ISR) and multiple-parton interactions (MPI) parameters to hadron collider data from the Tevatron and ATLAS. The tuning of Herwig/Jimmy is restricted to an MPI tune, cf. the MC10 tuning of that generator [5].

The tunes were performed using the stand-alone AGILe 1.2.0 event generator interface [6] to steer parameters and switches and to feed events to the Rivet 1.4.0 [7] analysis package. The parameter optimisation was done using the Professor 1.2.1 [8] tool.

1 Tuning of Pythia 6

The Pythia 6 [9] MC generator is used as the main general-purpose event generator in ATLAS. It is based, as are all general-purpose showering/hadronisation generators, on (leading-order) partonic matrix elements augmented with QCD radiation resummation via initial- and final-state parton showers, a non-perturbative model for the combination of the resultant partons into physical hadrons, a standard treatment of the decays of these hadrons, and – importantly for this note – a phenomenological modelling of the bulk interactions of the colliding protons via the formalism of multiple partonic interactions (MPI).

The hadronisation and MPI aspects of Pythia's event modelling are the most obvious targets for tuning to data, but as parton showers are accurate only to leading logarithmic accuracy and leading order splitting kernels are used, there is also some flexibility in e.g. the cutoff scale for their evolution. In this study, we attempt to optimise parameters in all these three areas of Pythia's event simulation.

ATLAS has for several years used Pythia 6 with a $p_\perp$-ordered parton shower. The previous shower, whose evolution was ordered in the virtuality of the emitted partons, had been extensively tuned at LEP [10] but the $p_\perp$-ordered shower parameters had only, until recently, been configured relatively roughly by the authors. As well as changing the shower evolution variable, the newer model as used by ATLAS also interleaves ISR emissions with MPI scatterings and reconnection of colour strings between MPI interactions. Until now, the ATLAS tunings of "$p_\perp$-ordered Pythia" have been confined to the parameters of this MPI model without regard for the initial state shower configuration [1, 11, 12]. The major motivation for the current extension of these tunings is the identification of a clear discrepancy between CDF and ATLAS transverse jet shape data [13, 14] and existing tunes of Pythia in its $p_\perp$-ordered mode. This discrepancy was addressed in the construction of the Perugia 2010 tune [15], whose base ISR configuration we adopt in this tuning.

For each tuning stage, several hundred points sampled from the Pythia parameter space were used to construct parameterisations and to obtain optimised parameter sets via the Professor MC tuning tool. All parameter samplings were uniform, parameter correlations are accounted for by use of cubic parameterisation functions, and quadrature-combined statistical and systematic errors have been used throughout. The fit weights were set *a priori* based on relevance to the model being tuned, the number of bins involved, and ATLAS' simulation priorities. They were then manually modified as required to balance the data description: this part of the optimisation procedure is unavoidably subjective. The final weights are tabulated in the following sections. The tune was performed in four stages following a similar approach to refs. [8, 15]:

1. Flavour parameters tuned to hadron multiplicities and their ratios, measured in e^+e^- collisions;
2. Final state radiation (FSR) and hadronisation parameters, tuned to event shapes and jet rates measured in e^+e^- collisions;
3. Initial state shower parameters and primordial k_T, tuned to Tevatron and LHC data;
4. Multiple-parton interactions, tuned to Tevatron and LHC data.

In the following, these four steps are described in separate sections. For this tune, the MRST LO** [16] PDF has been used. This PDF is a modified leading order PDF similar to the MRST LO* [17] one used in ATLAS' MC09 and MC10 simulation campaigns, with the distinction that the evolution of α_S in the PDF derivation is intended to scale with $p_\perp^2$, as is the case in event generator parton showers, rather than the more conventional Q^2. Aside from the motivation of having a "philosophically" more MC-oriented scale evolution, the use of the MRST LO** PDF has been chosen for this tune because its Λ_{QCD} value at 0.265 GeV is closer to that of a normal LO PDF than the comparatively high value of 0.345 in the LO* PDF: this is an important consideration for the ISR tuning stage, as discussed in section 1.3. An overview of all settings used for the tuning can be found in Table 5.

1.1 Flavour parameters

Pythia's hadronisation model has many parameters, including various approaches to affect the admixtures of hadron flavours (meson/baryon ratio, strangeness rates, η/η' ratio, etc.), orbitally excited states, and fragmentation kinematics. The flavour sector of the hadronisation was tuned to the same observables as in the flavour tuning described in ref. [8], and resulted in almost exactly the same parameter values as for that tune. In the interests of brevity in the current note, the reader is referred to that reference for details, but some representative plots are shown in Fig. 1.

Parameter i		$i_{\min}$	$i_{\max}$	A*T2	Default
PARJ(1)	Di-quark suppression	0.0	0.2	0.073	0.10
PARJ(2)	Strange suppression	0.1	0.4	0.2	0.30
PARJ(3)	Strange di-quark suppression	0.2	1.0	0.94	0.40
PARJ(4)	Spin-1 di-quark suppression	0.0	0.4	0.032	0.05
PARJ(11)	Spin-1 light meson	0.0	1.0	0.31	0.50
PARJ(12)	Spin-1 strange meson	0.0	1.0	0.4	0.60
PARJ(13)	Spin-1 heavy meson	0.0	1.0	0.54	0.75
PARJ(25)	η suppression	0.0	1.0	0.63	1.00
PARJ(26)	η' suppression	0.0	1.0	0.12	0.40

Table 1: Parameter sampling boundaries and tuned values of flavour parameters. The default values of these parameters were tuned for the Q^2-ordered rather than $p_\perp$-ordered parton shower, but were used with the latter in the ATLAS MC08, MC09 and AMBT1 Pythia tunes.

1.2 Final state radiation and hadronisation

The tuning of the kinematic aspects of final state showering and hadronisation, i.e. the distribution of energy and momentum in the emission of partons and in the formation of hadrons from partonic colour dipoles, was again pursued following the procedure used in the Professor study [8]. Our procedure differs from that previous tune in two major respects: we use much more data than in the Professor study, since several extra relevant analyses are now available in Rivet; and the Lund-Bowler heavy quark fragmentation parameter, PARP(47), is included with the light fragmentation parameters in this tune phase, rather than being tuned independently.

The Professor tune used only data from the DELPHI 1996 event shapes paper [10] and from the PDG Review of Particle Properties [19]. This study extends those input data sets to also include e^+e^- data from ALEPH, OPAL, and JADE, and in particular to place emphasis on several jet resolution variables, which probe the distribution of jets and their internal structure. This tuning of the FSR modelling to jet rates and event shapes applies at the LHC to the description of jet shapes in the decays of resonances like $Z/\gamma*$: while theoretically the same mechanism applies to *any* jets, Pythia 6 treats FSR from partons produced in an ISR process as distinct to FSR from matrix element outputs, and we optimise this description in the next section. The fit weights and observables used are listed in Table 3.

Observable	Weight
OPAL measurements $Z \to q\overline{q}$, $\sqrt{s} = 91.2$ **GeV** [18]	
b quark frag. function $f(x_B^{\text{weak}})$	1
Mean of b quark frag. function $f(x_B^{\text{weak}})$	1
uds events mean charged multiplicity	1
c events mean charged multiplicity	1
b events mean charged multiplicity	1
All events mean charged multiplicity	1
LEP particle multiplicities ($\sqrt{s} = 91.2$ **GeV**), taken from PDG [19]	
$\pi^{\pm}$ multiplicity	1
π^0 multiplicity	1
$\pi^0/\pi^{\pm}$ multiplicity ratio	6
$K^+/\pi^{\pm}$ multiplicity ratio	6
$K^0/\pi^{\pm}$ multiplicity ratio	6
$\eta/\pi^{\pm}$ multiplicity ratio	2
$\eta'(958)/\pi^{\pm}$ multiplicity ratio	1
$D^+/\pi^{\pm}$ multiplicity ratio	1
$D^0/\pi^{\pm}$ multiplicity ratio	1
$D_s^+/\pi^{\pm}$ multiplicity ratio	2
$(B^+, B_d^0)/\pi^{\pm}$ multiplicity ratio	1
$B^+/\pi^{\pm}$ multiplicity ratio	1
$B_s^0/\pi^{\pm}$ multiplicity ratio	2
$\rho^0(770)/\pi^{\pm}$ multiplicity ratio	9
$\rho^+(770)/\pi^{\pm}$ multiplicity ratio	9
$\omega(782)/\pi^{\pm}$ multiplicity ratio	9
$K^{*+}(892)/\pi^{\pm}$ multiplicity ratio	2
$K^{*0}(892)/\pi^{\pm}$ multiplicity ratio	2
$\phi(1020)/\pi^{\pm}$ multiplicity ratio	1
$D^{*+}(2010)/\pi^{\pm}$ multiplicity ratio	1
$D_s^{*+}(2112)/\pi^{\pm}$ multiplicity ratio	1
$B^*/\pi^{\pm}$ multiplicity ratio	1
$p/\pi^{\pm}$ multiplicity ratio	3
$\Lambda/\pi^{\pm}$ multiplicity ratio	4
$\Sigma^0/\pi^{\pm}$ multiplicity ratio	2
$\Sigma^{\pm}/\pi^{\pm}$ multiplicity ratio	2
$\Xi^-/\pi^{\pm}$ multiplicity ratio	1
$\Delta^{++}(1232)/\pi^{\pm}$ multiplicity ratio	1
$\Sigma^{\pm}(1385)/\pi^{\pm}$ multiplicity ratio	1

Table 2: Observable-weight combination used for the tuning of flavour parameters

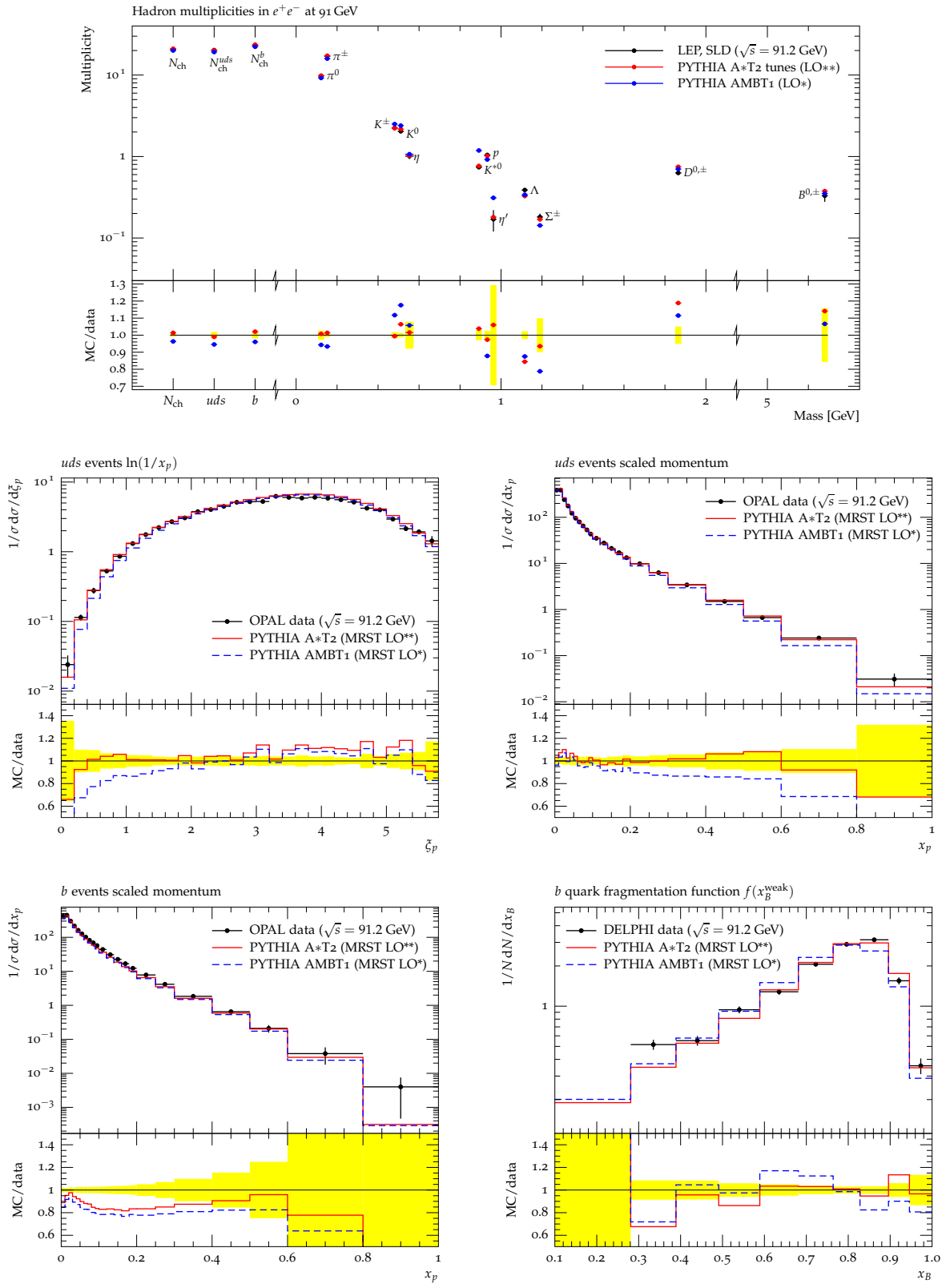

Figure 1: Comparison plots of the new Pythia 6 AMBT2/AUET2 tunes to LEP flavour-sensitive data.

Observable	Fit range	Weight
Studies of QCD with the ALEPH detector. [20]		
Scaled momentum, $x_p = \|p\|/\|p_{\text{beam}}\|$ (charged)		1
Rapidity w.r.t. thrust axes, y_T (charged)	$x \leq 4$	1
Rapidity w.r.t. thrust axes, y_T (charged)	$4 \leq x \leq 6$	5
In-plane p_T in GeV w.r.t. sphericity axes (charged)		1
Out-of-plane p_T in GeV w.r.t. sphericity axes (charged)	$1 \leq x \leq 3.5$	1
Mean π^0 multiplicity		10
Jet rates and event shapes at LEP I and II [21]		
Thrust minor ($E_{\text{CMS}} = 91.2$ GeV)	$\ln T_{\text{minor}} \leq -4.0$	5
Thrust minor ($E_{\text{CMS}} = 91.2$ GeV)	$-4.0 \leq \ln T_{\text{minor}} \leq -0.5$	2
Jet mass difference ($E_{\text{CMS}} = 91.2$ GeV)		1
Aplanarity ($E_{\text{CMS}} = 91.2$ GeV)		1
Oblateness ($E_{\text{CMS}} = 91.2$ GeV)		1
Sphericity ($E_{\text{CMS}} = 91.2$ GeV)		1
Thrust ($E_{\text{CMS}} = 91.2$ GeV)		1
Heavy jet mass ($E_{\text{CMS}} = 91.2$ GeV)		1
Total jet broadening ($E_{\text{CMS}} = 91.2$ GeV)		1
Wide jet broadening ($E_{\text{CMS}} = 91.2$ GeV)		1
C-Parameter ($E_{\text{CMS}} = 91.2$ GeV)		1
Thrust major ($E_{\text{CMS}} = 91.2$ GeV)		1
Delphi MC tuning on event shapes and identified particles. [10]		
In-plane $p_\perp$ in GeV w.r.t. thrust axes	$0 \leq x \leq 8$	2
In-plane $p_\perp$ in GeV w.r.t. thrust axes	$8 \leq x \leq 14$	6
Out-of-plane $p_\perp$ in GeV w.r.t. thrust axes	$0 \leq x \leq 1$	2
Out-of-plane $p_\perp$ in GeV w.r.t. thrust axes	$1 \leq x \leq 10$	10
Rapidity w.r.t. thrust axes, y_T		2
Rapidity w.r.t. sphericity axes, y_S		2
Scaled momentum, $x_p = \|p\|/\|p_{\text{beam}}\|$		2
$1 -$ Thrust		1
Thrust major, M		1
Thrust minor, m		1
Oblateness = $M - m$		1
Sphericity, S		1
Aplanarity, A		1
Planarity, P		1
C parameter		1
D parameter		1
Heavy hemisphere masses, M_h^2/E_{vis}^2		1
Light hemisphere masses, M_l^2/E_{vis}^2		1
Difference in hemisphere masses, M_d^2/E_{vis}^2		1
Wide hemisphere broadening, B_{max}		1
Narrow hemisphere broadening, B_{min}		1
Total hemisphere broadening, B_{sum}		1
Difference in hemisphere broadening, B_{diff}		1
Differential 3-jet rate with Durham algorithm, D_2^{Durham}		1
Differential 4-jet rate with Durham algorithm, D_3^{Durham}		1
Differential 5-jet rate with Durham algorithm, D_4^{Durham}		1
Energy-energy correlation, EEC		1
Asymmetry of the energy-energy correlation, AEEC		1
Mean charged multiplicity		5000
Study of the b-quark fragmentation function at LEP 1 [22]		
b quark fragmentation function $f(x_B^{\text{weak}})$	$0.25 \leq x \leq 1.0$	10

continued on next page

Observable	Fit range	Weight
Mean of b quark fragmentation function $f(x_B^{\text{weak}})$		5
Jet rates in e^+e^- at JADE [35–44 GeV] and OPAL [91–189 GeV]. [23]		
Integrated 2-jet rate with Durham algorithm (91.2 GeV)		4
Integrated 3-jet rate with Durham algorithm (91.2 GeV)		4
Integrated 4-jet rate with Durham algorithm (91.2 GeV)		4
Integrated 5-jet rate with Durham algorithm (91.2 GeV)		4
Integrated $\geq$6-jet rate with Durham algorithm (91.2 GeV)		4
Differential 2-jet rate with Durham algorithm (91.2 GeV)		4
Differential 3-jet rate with Durham algorithm (91.2 GeV)		4
Differential 4-jet rate with Durham algorithm (91.2 GeV)		4
Differential 5-jet rate with Durham algorithm (91.2 GeV)		4
Measurements of flavor dependent fragmentation functions in $Z^0 -> q\bar{q}$ events [18]		
uds events scaled momentum		10
uds events mean charged multiplicity		500
Hadron multiplicities in hadronic e^+e^- events [19]		
Mean π^+ multiplicity		500
Mean π^0 multiplicity		500

Table 3: Observable-weight combination used for the tuning of FSR and hadronisation parameters

Parameter i		i_{min}	i_{max}	A*T2	Default
PARJ(21)	σ_{string}	0.20	0.45	0.30	0.36
PARJ(41)	Lund_a	0.1	1.8	0.368	0.30
PARJ(42)	Lund_b	0.2	2.5	1.004	0.58
PARJ(47)	Bowler-fragmentation (for heavy quarks)	0.0	1.5	0.873	1.00
PARJ(81)	Λ_{QCD}	0.18	0.32	0.256	0.29
PARJ(82)	Shower cut-off	0.4	2.0	0.830	1.00

Table 4: Parameter sampling boundaries and tuned values of FSR and hadronisation parameters. The default values of these parameters were tuned for the Q^2-ordered rather than $p_\perp$-ordered parton shower, but were used with the latter in the ATLAS MC08, MC09 and AMBT1 Pythia tunes.

Switch		A*T2
MSTP(52)	Use LHAPDF for external PDFs	2
MSTP(51)	Use MRST LO** PDF	20651
MSTJ(11)	Bowler-fragmentation function for heavy quarks	5
MSTJ(41)	$p_\perp$-ordered shower	12
MSTP(70)	ISR regularisation scheme with cut-off at PARP(62)/2	0
MSTP(64)	Set α_S scheme for ISR to CMW [b)]	3
MSTP(72)	Allow colour dipoles stretched between ISR dipoles to radiate FSR	2
MSTP(3)	Allow different α_S for different shower parts [a)]	1
MSTU(112)	Set number of flavours considered in α_S expression	4
PARU(112)	Set Λ in α_S running coupling calculation algorithm to Λ in PDF	0.265
PARP(1)	Set Λ_{QCD} in running α_S for hard scattering to Λ in PDF	0.265
PARP(61)	Set Λ_{QCD} in running α_S for ISR to Λ in PDF	0.265

[a)] Λ is given by PARP(1) for hard interactions, by PARP(61) for ISR, by PARP(72) for FSR not from a resonance decay, and by PARJ(81) for FSR from a resonance decay

[b)] This setting was introduced in Pythia 6.419 and therefore undocumented in the Pythia 6 manual. The release notes of Pythia 6 refer to [24].

Table 5: Switches and fixed parameter values used for tuning of Pythia 6.

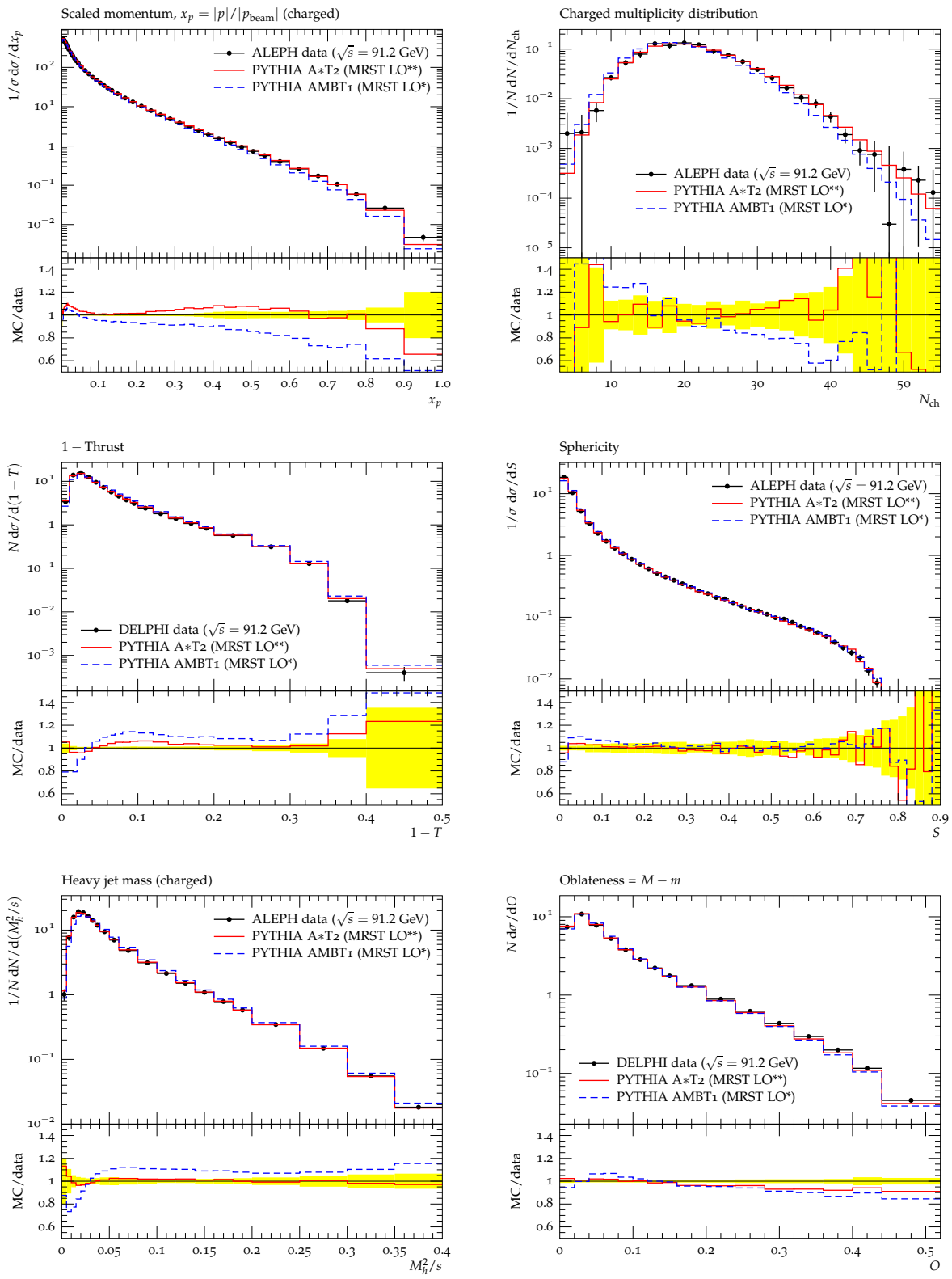

Figure 2: Comparison plots of the new Pythia 6 AMBT2/AUET2 tunes to LEP event shape data.

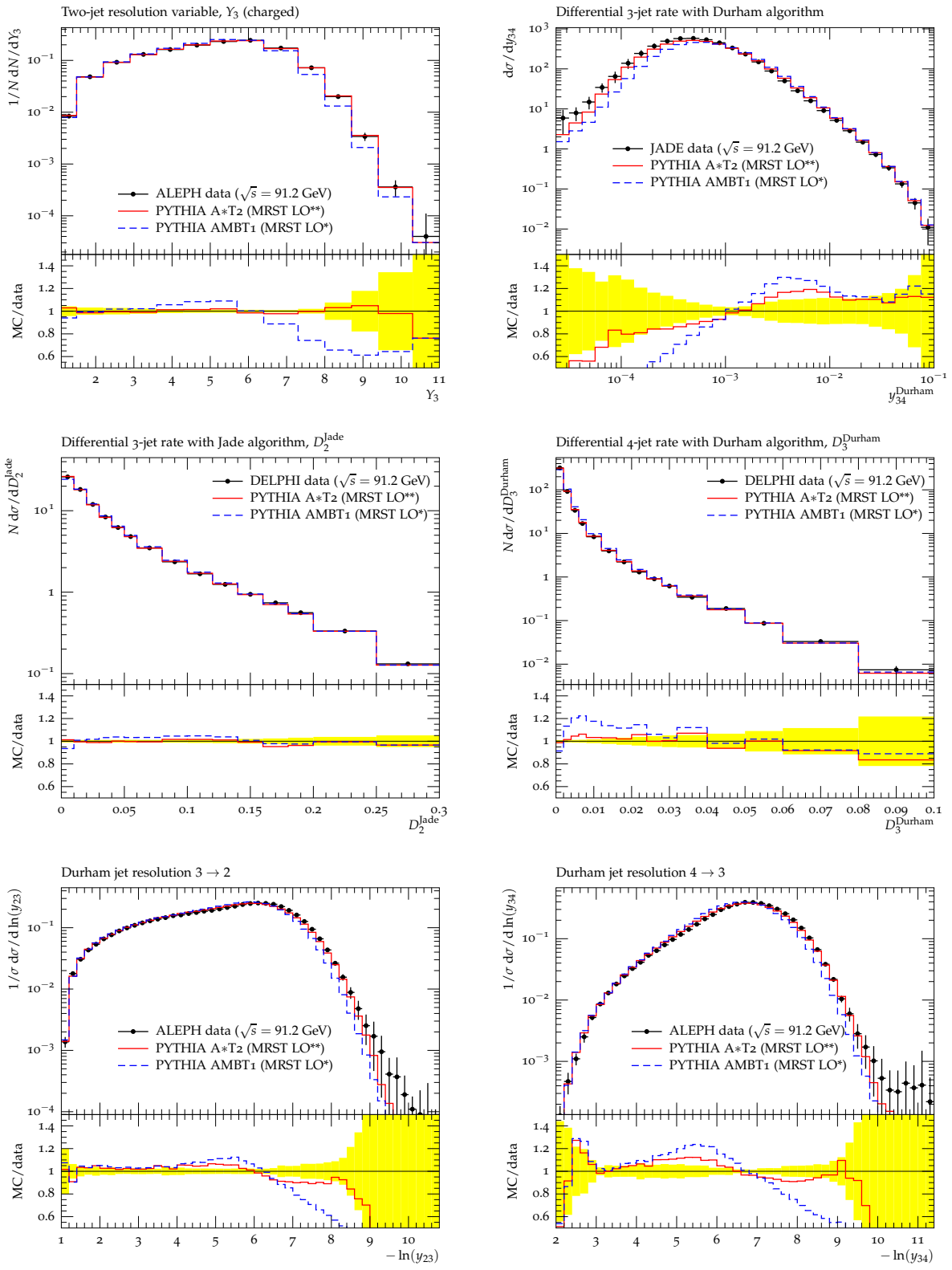

Figure 3: Comparison plots of the new Pythia 6 AMBT2/AUET2 tunes to LEP jet data.

1.3 Initial state radiation and primordial k_T

The ATLAS measurement of the jet shapes in events containing at least one jet above 20 GeV revealed that the AMBT1 tune predicts jets which are too narrow. Similar behaviour had been observed when comparing the Perugia 0 tune to jet shape data measured at the Tevatron and a new tune Perugia 2010 was developed to improve the description, this tune turned out to also describe the ATLAS jet shapes data better. The main goal of tuning the shower parameters is to achieve a better description of these data within ATLAS' chosen PDFs and models.

Pythia provides possibilities to change both Λ_{QCD} in the definition of the α_S evolution for ISR and the allowed phase space for ISR radiation. The strong coupling in the ISR shower is defined as $\alpha_S(kQ/\Lambda^2_{\mathrm{ISR}})$ where the multiplicative factor k is specified in the Pythia model by the PARP(64) parameter, and the QCD scale Λ_{ISR} is given by PARP(61). For this tune, we follow the Perugia 2010 tune strategy and set PARP(61) $= 0.265$, i.e. to the nominal Λ_{QCD} value in the LO** PDF. PARP(64) is used as a free parameter for tuning.

Pythia 6 also provides the possibility to use either the $\overline{\mathrm{MS}}$ or the CMW [24] representation of Λ_{QCD} for the ISR evolution. The effective distinction of the two schemes is that the CMW scheme multiplies the Λ_{QCD} in ISR by a factor of approximately 1.6. The exact scale factor depends on the number of active flavours [25]: for this tune we followed the Perugia 2010 tune by using the CMW scheme, and the applied 4-flavour scale factor is $\Lambda_4^{\mathrm{CMW}} = 1.618 \cdot \Lambda_4^{\overline{\mathrm{MS}}}$. Due to this treatment, and the explicit setting of Λ_{QCD} to match the LO** PDF value, the initial-state Λ_{QCD} values used in this tune are significantly higher than in previous tunes.

The remaining ISR parameters are PARP(62), which specifies the lowest $p_\perp$ value to which the shower will evolve before terminating, and PARP(67), which is a multiplicative scale factor applied to the maximum scale at which the shower begins its evolution. Both of these parameters are optimised by tuning.

A key element of this tuning from the point of view of jet shapes is the Λ_{QCD} value used calculating α_S in FSR showers starting from ISR partons. This is specified by $\Lambda^{\mathrm{IFSR}}_{\mathrm{QCD}} = $ PARP(72), and its value is expected to be more "FSR-like" than "ISR-like", based on the experience from Perugia 2010. While the good agreement with jet shape data found in that tune by setting PARP(72) to the Λ_{QCD} value from hadronisation bodes well for the effect of our second tuning stage, we consider the jet shape descriptions sufficiently important for ATLAS physics to tune this parameter explicitly to ATLAS and Tevatron data, rather than simply setting it to the value found by tuning to e^+e^- observables.

The final parameter in this tune stage is the distribution of primordial k_T inside the hadron: in Pythia, as in all other current event generators, this is modelled by a Gaussian distribution, with the energy-independent width $\sigma = $ PARP(91) as a tuneable parameter. While this variable only has a major impact on the low-$p_\perp$ part of well-defined $p_\perp$ distributions, e.g. the position of the peak of the Z^0 boson $p_\perp$ spectrum in Drell-Yan events, we include it together with the shower parameters in this tune to empirically assess the degree of correlation with shower variables and to account for any which are found.

1.3.1 Data sets used for tuning

The shapes of jets measured in inclusive jet production by the ATLAS and CDF experiments and the fragmentation function of track jets measured by ATLAS [26] are particularly sensitive to these shower parameters, and hence had most impact on the optimised value of the shower parameters. During the tuning, a small tension between the track fragmentation function and the jet shapes was observed in the sense that the track fragmentation function would better be described with lower values of PARP(72), while the jet shapes pull to higher values.

The azimuthal decorrelation data measured by ATLAS [27] show sensitivity to the parameter PARP(67).

This parameter is of particular interest, as it is used to estimate systematic uncertainty of jets created by ISR in measurements at high-$p_\perp$, e.g. top pair production. However, it should be noted, that due to the different implementation details for the shower in dijet events with low mass jets and the shower in events with top pair production, the results obtained by tuning to dijet data cannot be interpreted as limits for the uncertainty on ISR for these high-$p_\perp$ processes.

The value of the primordial k_T is almost solely determined by the shape and position of the peak of the Z^0 $p_\perp$ spectrum. The high $p_\perp$ part of the Z^0 $p_\perp$ spectrum is sensitive to the modelling of the ISR radiation. Since these parameter sensitivities cannot be entirely separated in this observable, the tuning of primordial k_T is included in the ISR tuning.

1.3.2 Tuning and results

The datasets and parameter ranges used for this tuning are listed in Table 6; this 5 parameter tune used 300 MC runs for the Professor parameterisation. The weights apply a higher emphasis on the ATLAS data than on that from the Tevatron. The AMBT1 tune's MPI configuration was used as a base for this ISR tuning: due to the change of PDF, this is not ideal, but was chosen to give a level of MPI activity which was not greatly different from data without a need for a cyclic iteration of the ISR and MPI tune stages.

Figures 4,5, 6 and 7 show the data distributions used for tuning compared to the optimised parameter setting. For these comparisons the optimised parameters of all tuning steps, including the MPI stage which is described in the next section. A description of the ATLAS jet shape data is achieved within 5% for jets up to $p_\perp$ of 300 GeV which is an improvement compared to AMBT1 where up to 15% disagreement with these data were found. However, the jet shapes measured by CDF at 1.96 TeV still show up to 20% disagreement in some regions. The track jet fragmentation function is well-described, with the MC prediction undershooting the data at high z by about 10% . There was an evident tension between the transverse jet shape and longitudinal fragmentation function data, and the fit weights were chosen to give what was considered to be a balanced description of both data types. The azimuthal dijet decorrelation data are described to within the experimental uncertainty.

Observable	$\sqrt{s}$	Fit range	Weight
ATLAS jet shapes [14]			
Diff. jet shapes [a)] ρ for $p_\perp \in [30,40]$ GeV	7 TeV		1
Diff. jet shapes [a)] ρ for $p_\perp \in [40,60]$ GeV	7 TeV		1
Diff. jet shapes [a)] ρ for $p_\perp \in [60,80]$ GeV	7 TeV		1
Diff. jet shapes [a)] ρ for $p_\perp \in [80,110]$ GeV	7 TeV		1
Diff. jet shapes [a)] ρ for $p_\perp \in [110,160]$ GeV	7 TeV		1
Diff. jet shapes [a)] ρ for $p_\perp \in [160,210]$ GeV	7 TeV		1
Diff. jet shapes [a)] ρ for $p_\perp \in [210,260]$ GeV	7 TeV		1
Diff. jet shapes [a)] ρ for $p_\perp \in [260,310]$ GeV	7 TeV		1
Diff. jet shapes [a)] ρ for $p_\perp \in [310,400]$ GeV	7 TeV		1
Diff. jet shape ρ for $p_\perp \in [400,500]$ GeV, $y \in [0.0,2.8]$	7 TeV		5
Diff. jet shape ρ for $p_\perp \in [500,600]$ GeV, $y \in [0.0,2.8]$	7 TeV		5
ATLAS dijet decorrelations [27]			
$\Delta\phi_{12}$, $110 < p_\perp^{\max} < 160$ GeV	7 TeV		5
$\Delta\phi_{12}$, $160 < p_\perp^{\max} < 210$ GeV	7 TeV		5
$\Delta\phi_{12}$, $210 < p_\perp^{\max} < 310$ GeV	7 TeV	$2.1 \leq \Delta\phi_{12} \leq \pi$	5
$\Delta\phi_{12}$, $p_\perp^{\max} < 310$ GeV	7 TeV	$2.3 \leq \Delta\phi_{12} \leq \pi$	5
ATLAS track jets [26]			
Longit. jet frag. function, z for $p_\perp^{\text{jet}} \in [4,6]$ GeV, $R = 0.4$	7 TeV		5
Longit. jet frag. function, z for $p_\perp^{\text{jet}} \in [6,10]$ GeV, $R = 0.4$	7 TeV		5
Longit. jet frag. function, z for $p_\perp^{\text{jet}} \in [10,15]$ GeV, $R = 0.4$	7 TeV		5
Longit. jet frag. function, z for $p_\perp^{\text{jet}} \in [15,24]$ GeV, $R = 0.4$	7 TeV		5
ATLAS W plus jets [28]			
1^{st} jet $p_\perp$ (electron channel)	7 TeV	$p_\perp > 40$ GeV	5
1^{st} jet $p_\perp$ (muon channel)	7 TeV	$p_\perp > 40$ GeV	5
CDF Z^0 $p_\perp$ and total cross-section in $Z \to e^+e^-$ [29]			
$p_\perp(Z^0)$	1800 GeV	$p_\perp < 10$ GeV	6
CDF jet shapes [13]			
Differential jet shapes [b)] $\rho(r/R)$	1960 GeV		1
D0 dijet ϕ decorrelations [30]			
$\Delta\phi_{12}$, $p_\perp^{\max} \in [75,100]$ GeV	1960 GeV		2
$\Delta\phi_{12}$, $p_\perp^{\max} \in [100,130]$ GeV	1960 GeV		2
$\Delta\phi_{12}$, $p_\perp^{\max} \in [130,180]$ GeV	1960 GeV		2
$\Delta\phi_{12}$, $p_\perp^{\max} > 180$ GeV	1960 GeV		2

[a)] This observable enters the fit for five different, non-overlapping rapidity windows with the same weight: $y \in$ $[0.0,0.3]$, $[0.3,0.8]$, $[0.8,1.2]$, $[1.2,2.1]$, $[2.1,2.8]$

[b)] A total of 18 ρ distributions with different, non-overlapping windows for the jet-$p_\perp$ from 37 to 380 GeV entered the fit. All had the same weight assigned.

Table 6: Observables and tuning weights used for tuning of the Pythia shower and intrinsic k_T parameters.

Description	Pythia Parameter	Tuning range	optimised value	AMBT1	Perugia 2010
ISR cut-off	PARP(62)	1.75–3.0	2.80	1.025	1.0
ISR scale factor on α_S eval. scale	PARP(64)	1.0–2.5	2.21	1.0	1.0
Scaling of max. parton virtuality	PARP(67)	0.1–2.0	0.66	4.0	1.0
Λ_{QCD} for FSR off ISR	PARP(72)	0.1–0.4	0.25	0.192	0.26
Primordial k_T	PARP(92)	0.8–2.5	1.92	2.0	2.0

Table 7: Shower and intrinsic k_T parameters used in the tune, the optimised parameters for the new tunes AMBT2 and AUET2, labelled as A*T2 here, and a comparison to previous ATLAS tune and Perugia 2010 settings. For a comparison of the specific value of PARP(64), it should be noted that the specific setting of PARP(61) and the Λ scheme has to be taken into account. In particular, for AMBT1: PARP(61) $= 0.192$, and $\Lambda_{\overline{\mathrm{MS}}}$; and for Perugia 2010, Λ_{CMW} and PARP(61) $= 0.192$

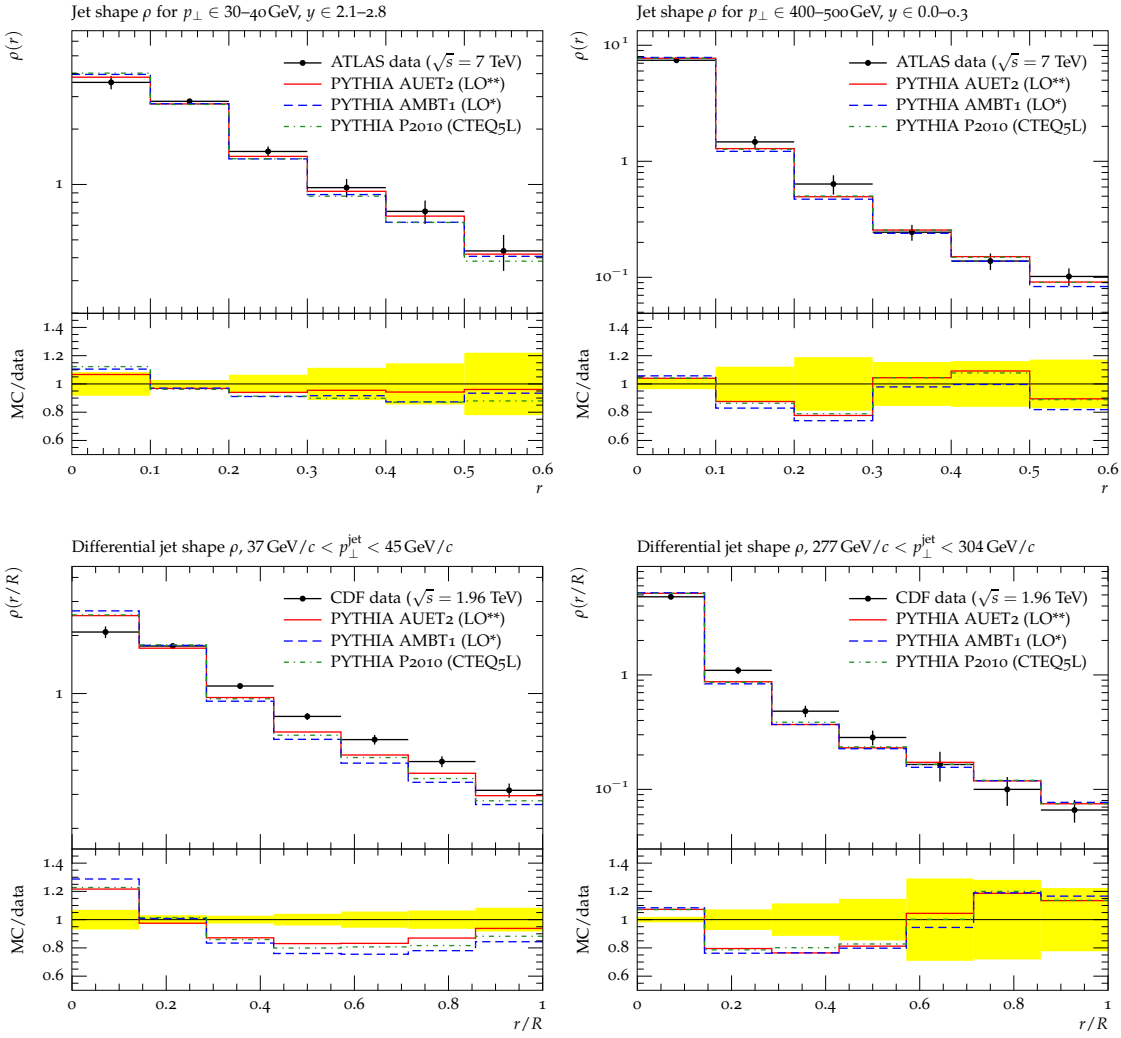

Figure 4: Comparison of the new tune AUET2 Pythia tune to jet shape measurements from ATLAS (upper row) and CDF (lower row).

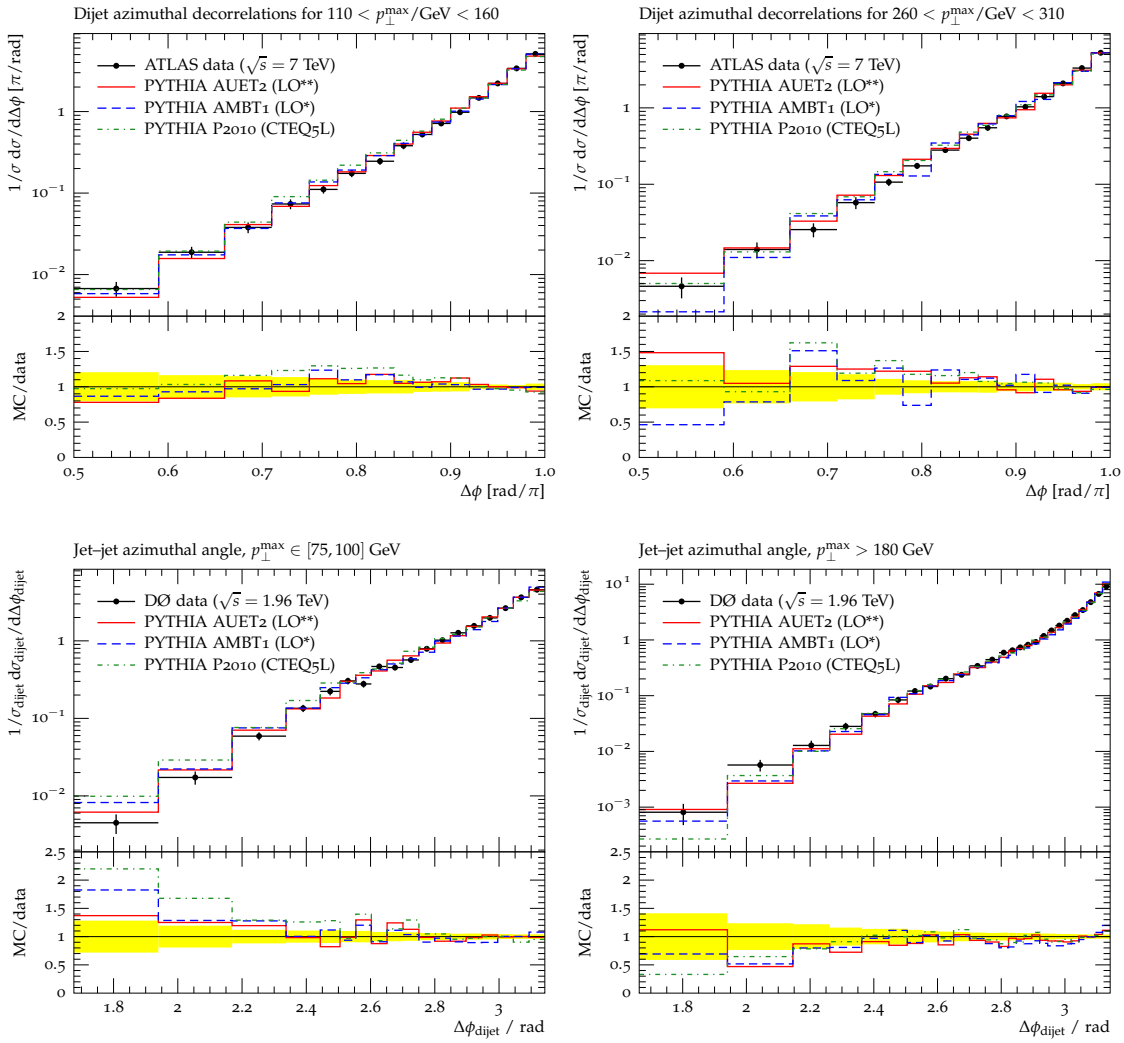

Figure 5: Comparison of the new AUET2 Pythia tune to dijet azimuthal decorrelations measured by ATLAS (upper row) and DØ (lower row). These comparisons are shown for the lowest (left) and highest (right) $p_\perp$ bins. The preliminary versions of the ATLAS observables, with lower-statistics, were used in the tune.

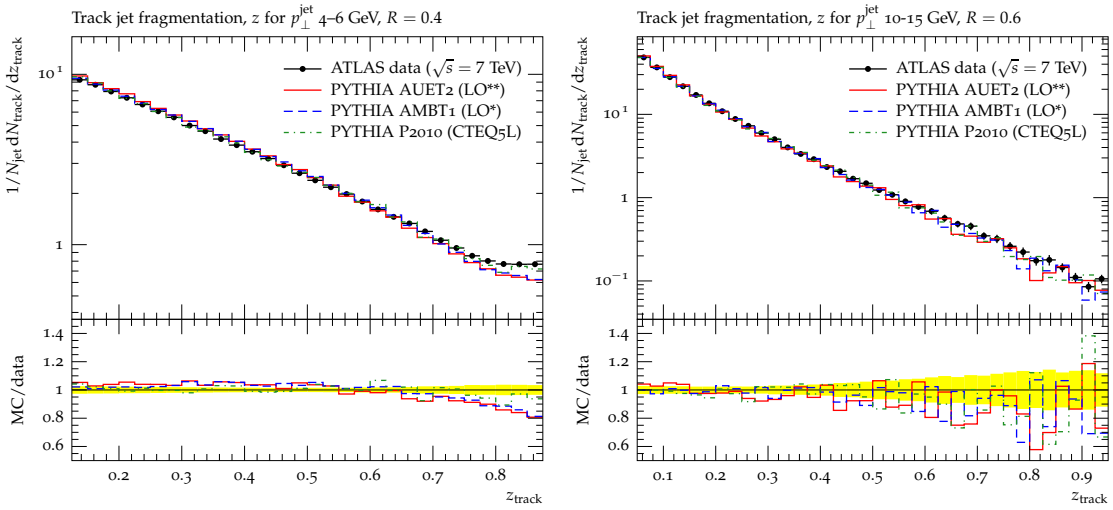

Figure 6: Comparison of the new AUET2 Pythia tune to ATLAS measurements of the track jet fragmentation for a k_T track jet radius of $R = 0.4$

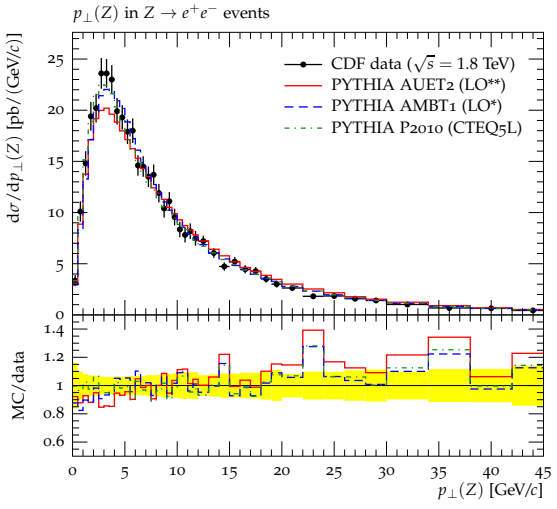

Figure 7: Comparison of the new AUET2 Pythia tune to the $p_\perp$ distribution of $Z^0 \to e^+e^-$ events as measured by CDF.

1.4 Multiple parton interactions

The final stage of tuning is the same as that considered in previous ATLAS tunes of Pythia: the parameters of the multiple-parton interaction model are optimised. This part of Pythia's event modelling is less constrained by robust theory than other aspects, and accordingly it is placed last in the tuning sequence to minimise the amount of freedom available in its tuning: had we placed the MPI tuning earlier than that of ISR, the MPI modelling would have attempted to compensate for the features of the untuned ISR model, and the eventual result would have been less optimal.

Multiple parton interactions and their modelling in Pythia (and Jimmy) have been discussed in many previous papers and notes [1, 9, 11, 31], so we merely review the parameters. The $p_\perp$ cutoff/regulariser value used to avoid soft divergences in the model, set for a reference scale of $\sqrt{s} = 1800$ GeV, and the exponent used in its energy evolution to other beam energies are given by PARP(82) and PARP(90) respectively: both are included in the tune. The hadronic matter distribution is modelled by a double-Gaussian distribution, parametrised by PARP(83) and PARP(84): as these parameters are strongly correlated, we fixed PARP(83) to its AMBT1 value of 0.356 and only tuned PARP(84). The final parameters are PARP(77) and PARP(78), which control the probabilities of colour reconnection occurring for fast-moving (high-$p_\perp$) and general colour strings: both are tuned. The final sampling ranges used for these parameters are shown in Table 8, and the observables and weights are shown in Tables 9 and 10.

The production of observables for this phase of the tuning required several extensions of the initial tuning ranges, particularly because the ATLAS minimum bias observables wished to set the PARP(82) and PARP(78) parameters beyond the upper and lower boundaries of the initial sampling ranges respectively. As a result, many more runs were used than in the other stages: a total of 553 runs were made and used for the final tuning. The required range extension, particularly in PARP(82), is thought to be related to a recently discovered bug in LHAPDF, which reports a $\Lambda_{\rm QCD}$ value of 0.192 for all PDFs: hence all tunes of Pythia in which no explicit value of $\Lambda_{\rm QCD}$ was set for the ISR and MPI were using 0.192 rather than the true PDF value. This explains the previous lack of variation between PDFs for jet shape observables, which are very sensitive to $\Lambda^{\rm IFSR}_{\rm QCD}$ as described in the previous section. In this tune, we explicitly set the ISR/MPI $\Lambda_{\rm QCD}$ values to the true PDF value of 0.265, and hence the α_S used in MPI scatterings is higher than "normal" and more screening of the MPI soft cross-section divergence (higher PARP(82) – see MPI model summary references) is required to match the ATLAS minimum bias normalisation.

Several variations of fit weights were explored before settling on final tunes, as it was found to be impossible to simultaneously describe all the desired observables. In particular, including both ATLAS minimum bias and underlying even observables led to MC–data discrepancies of order 20% in levels of $N_{\rm ch}$ and $\sum p_\perp$ activity, and the range of ATLAS underlying event $p_{\rm T}^{\rm lead}$ bins in the fit had to be restricted to only use the plateau regions. The most satisfactory results were obtained by separate tuning to minimum bias and UE observables, and hence we are forced to provide two distinct tunes: AMBT2, tuned to the minimum bias data only, and AUET2, tuned only to UE data. The major differences between these two tunes, whose parameters are given in Table 8, lie in the colour reconnection parameters, PARP(77) and PARP(78).

The two most difficult analyses to describe in conjunction with all others are the ATLAS minimum bias analysis, which apparently requires a level of MPI activity much less than that the UE observables constructed on the same dataset, and the CDF Run II leading jets UE analysis, which requires a level of MPI activity lower than that in the other CDF UE analyses at the same (or nearly the same) energy. Tuning to the ATLAS minimum bias observables separately from almost all others hence resolves the first discrepancy, but the poor description of the CDF leading jets UE is evident in the final AUET2 tune, in Fig. 14 – while other CDF UE observables are fairly well described. We also note in passing that the quality of UE observable fit is very similar to that of Perugia 2010, and in particular that the transition from the "ramp" to "plateau" regions in the UE profiles significantly undershoots the data. It is possible that these unresolvable discrepancies stem from the tuning of the ISR, and in particular from the very different treatment of $\Lambda_{\rm QCD}$

Description	Pythia Parameter	Tuning range	AMBT2	AUET2	AMBT1	Perugia 2010
Fast string CR	PARP(77)	0.25–1.15	0.88	1.12	1.02	1.00
CR strength	PARP(78)	0.1–0.6	0.18	0.33	0.54	0.35
$p_{\perp}^{0}(\sqrt{s} = 1800\ \text{GeV})$	PARP(82)	2.1–2.7	2.49	2.45	2.29	2.05
Matter distribution	PARP(84)	0.0–1.0	0.62	0.53	0.65	– [a)]
$p_{\perp}^{0}$ $\sqrt{s}$ evolution exponent	PARP(90)	0.18–0.28	0.244	0.229	0.250	0.26

[a)] Perugia 2010 uses a exponential matter distribution which doesn't use this parameter.

Table 8: MPI parameters used in the tunes, the optimised parameters and a comparison to previous ATLAS tune and Perugia 2010 settings. The Perugia 2010 tune used a PARP(83) value of 1.5, as opposed to the AMBT1 value of 0.356 used in all the other tunes shown here.

in this setup as compared to previous tunes where a value of 0.192 was unintentionally being used: future tuning attempts will try to be more consistent in the use of Λ_{QCD}, and it would also be desirable to combine the ISR and MPI tuning phases – although this raises many technical issues relating to the much-increased dimensionality of the tuning space: this may hence require a multi-stage rough/fine combined tune.

A final comment is worthwhile regarding the AMBT2 tune: it may be seen in Figures 8 and 9 that the low (and statistically dominant) end of the charged multiplicity spectrum is improved in AMBT2 over AMBT1, but that the high multiplicities are not so well described: which is more important in a minimum bias tune is a matter of opinion, and hence AMBT2 makes an interesting systematic partner to AMBT1 rather than an unconditional improvement. Similarly, the description of the $p_{\perp}$ spectra is more deviant than in other tunes. By varying the MPI parameters and greatly increasing the fit weights on the $p_{\perp}$ spectrum, it was found to be impossible to improve the quality of this fit: we suspect that again this observable is dominated by shower effects, and perhaps again the effect of the Λ_{QCD} treatment in these tunes. These features will be investigated in future tuning studies, but it is evident that at least in the setup on which these tunes are based, Pythia is unable to simultaneously describe not just all features of the available data, but not even all features of minimum bias or UE data in isolation.

Observable	$\sqrt{s}$	Weight
Track-based minimum bias at 900 GeV and 7 TeV in ATLAS [1]		
N_{ch}, track $p_\perp > 2500$ MeV, $N_{\text{ch}} \geq 1$	7 TeV	20
$p_\perp$, track $p_\perp > 2500$ MeV, $N_{\text{ch}} \geq 1$	7 TeV	20
η, track $p_\perp > 2500$ MeV, $N_{\text{ch}} \geq 1$	7 TeV	20
$\langle p_\perp \rangle$ vs. N_{ch}, track $p_\perp > 2500$ MeV, $N_{\text{ch}} \geq 1$	7 TeV	20
N_{ch}, track $p_\perp > 500$ MeV, $N_{\text{ch}} \geq 6$	7 TeV	40
$p_\perp$, track $p_\perp > 500$ MeV, $N_{\text{ch}} \geq 6$	7 TeV	40
η, track $p_\perp > 500$ MeV, $N_{\text{ch}} \geq 6$	7 TeV	40
$\langle p_\perp \rangle$ vs. N_{ch}, track $p_\perp > 500$ MeV, $N_{\text{ch}} \geq 6$	7 TeV	30
N_{ch}, track $p_\perp > 100$ MeV, $N_{\text{ch}} \geq 20$	7 TeV	10
$p_\perp$, track $p_\perp > 100$ MeV, $N_{\text{ch}} \geq 20$	7 TeV	10
η, track $p_\perp > 100$ MeV, $N_{\text{ch}} \geq 20$	7 TeV	10
$\langle p_\perp \rangle$ vs. N_{ch}, track $p_\perp > 100$ MeV, $N_{\text{ch}} \geq 20$	7 TeV	10
N_{ch}, track $p_\perp > 2500$ MeV, $N_{\text{ch}} \geq 1$	900 GeV	10
$p_\perp$, track $p_\perp > 2500$ MeV, $N_{\text{ch}} \geq 1$	900 GeV	10
η, track $p_\perp > 2500$ MeV, $N_{\text{ch}} \geq 1$	900 GeV	10
$\langle p_\perp \rangle$ vs. N_{ch}, track $p_\perp > 2500$ MeV, $N_{\text{ch}} \geq 1$	900 GeV	10
N_{ch}, track $p_\perp > 500$ MeV, $N_{\text{ch}} \geq 6$	900 GeV	20
$p_\perp$, track $p_\perp > 500$ MeV, $N_{\text{ch}} \geq 6$	900 GeV	20
η, track $p_\perp > 500$ MeV, $N_{\text{ch}} \geq 6$	900 GeV	20
$\langle p_\perp \rangle$ vs. N_{ch}, track $p_\perp > 500$ MeV, $N_{\text{ch}} \geq 6$	900 GeV	15
N_{ch}, track $p_\perp > 100$ MeV, $N_{\text{ch}} \geq 20$	900 GeV	5
$p_\perp$, track $p_\perp > 100$ MeV, $N_{\text{ch}} \geq 20$	900 GeV	5
η, track $p_\perp > 100$ MeV, $N_{\text{ch}} \geq 20$	900 GeV	5
$\langle p_\perp \rangle$ vs. N_{ch}, track $p_\perp > 100$ MeV, $N_{\text{ch}} \geq 20$	900 GeV	5
CDF Run II minimum bias [32]		
$\langle p_\perp \rangle$ vs. N_{ch}	1960 GeV	5

Table 9: Observable–weight combinations used for the AMBT2 MPI tuning.

Observable	$\sqrt{s}$	Fit range	Weight
Track-based underlying event at 900 GeV and 7 TeV in ATLAS [2]			
Transverse region N_{chg} density vs. $p_\perp$ (leading track)	7 TeV	$\geq$ 6 GeV	40
Toward region N_{chg} density vs. $p_\perp$ (leading track)	7 TeV	$\geq$ 6 GeV	10
Away region N_{chg} density vs. $p_\perp$ (leading track)	7 TeV	$\geq$ 6 GeV	10
Transverse region $\sum p_\perp$ density vs. $p_\perp$ (leading track)	7 TeV	$\geq$ 6 GeV	40
Toward region $\sum p_\perp$ density vs. $p_\perp$ (leading track)	7 TeV	$\geq$ 6 GeV	10
Away region $\sum p_\perp$ density vs. $p_\perp$ (leading track)	7 TeV	$\geq$ 6 GeV	10
Transverse region $\langle p_\perp \rangle$ density vs. $p_\perp$ (leading track)	7 TeV		40
Toward region $\langle p_\perp \rangle$ density vs. $p_\perp$ (leading track)	7 TeV		10
Away region $\langle p_\perp \rangle$ density vs. $p_\perp$ (leading track)	7 TeV		10
Transverse region $\langle p_\perp \rangle$ density vs. N_{ch} (leading track)	7 TeV		40
Toward region $\langle p_\perp \rangle$ density vs. N_{ch} (leading track)	7 TeV		10
Away region $\langle p_\perp \rangle$ density vs. N_{ch} (leading track)	7 TeV		10
Transverse region N_{chg} density vs. $p_\perp$ (leading track), $p_\perp > 100$ MeV	7 TeV		10
Toward region N_{chg} density vs. $p_\perp$ (leading track), $p_\perp > 100$ MeV	7 TeV		4
Away region N_{chg} density vs. $p_\perp$ (leading track), $p_\perp > 100$ MeV	7 TeV		4
Transverse region $\sum p_\perp$ density vs. $p_\perp$ (leading track), $p_\perp > 100$ MeV	7 TeV		10
Toward region $\sum p_\perp$ density vs. $p_\perp$ (leading track), $p_\perp > 100$ MeV	7 TeV		4
Away region $\sum p_\perp$ density vs. $p_\perp$ (leading track), $p_\perp > 100$ MeV	7 TeV		4
Transverse region N_{chg} density vs. $p_\perp$ (leading track)	900 GeV	$\geq$ 3 GeV	20
Toward region N_{chg} density vs. $p_\perp$ (leading track)	900 GeV	$\geq$ 3 GeV	5
Away region N_{chg} density vs. $p_\perp$ (leading track)	900 GeV	$\geq$ 3 GeV	5
Transverse region $\sum p_\perp$ density vs. $p_\perp$ (leading track)	900 GeV	$\geq$ 3 GeV	20
Toward region $\sum p_\perp$ density vs. $p_\perp$ (leading track)	900 GeV	$\geq$ 3 GeV	5
Away region $\sum p_\perp$ density vs. $p_\perp$ (leading track)	900 GeV	$\geq$ 3 GeV	5
Transverse region $\langle p_\perp \rangle$ density vs. $p_\perp$ (leading track)	900 GeV		20
Toward region $\langle p_\perp \rangle$ density vs. $p_\perp$ (leading track)	900 GeV		5
Away region $\langle p_\perp \rangle$ density vs. $p_\perp$ (leading track)	900 GeV		5
Transverse region $\langle p_\perp \rangle$ density vs. N_{ch} (leading track)	900 GeV		20
Toward region $\langle p_\perp \rangle$ density vs. N_{ch} (leading track)	900 GeV		5
Away region $\langle p_\perp \rangle$ density vs. N_{ch} (leading track)	900 GeV		5
Transverse region N_{chg} density vs. $p_\perp$ (leading track), $p_\perp > 100$ MeV	900 GeV		5
Toward region N_{chg} density vs. $p_\perp$ (leading track), $p_\perp > 100$ MeV	900 GeV		2
Away region N_{chg} density vs. $p_\perp$ (leading track), $p_\perp > 100$ MeV	900 GeV		2
Transverse region $\sum p_\perp$ density vs. $p_\perp$ (leading track), $p_\perp > 100$ MeV	900 GeV		5
Toward region $\sum p_\perp$ density vs. $p_\perp$ (leading track), $p_\perp > 100$ MeV	900 GeV		2
Away region $\sum p_\perp$ density vs. $p_\perp$ (leading track), $p_\perp > 100$ MeV	900 GeV		2
Cluster-based underlying event at 900 GeV and 7 TeV in ATLAS [3]			
Transverse N density vs. $p_\perp^{\text{clus1}}$	7 TeV		20
Transverse $\sum p_\perp$ density vs. $p_\perp^{\text{clus1}}$	7 TeV		20
Transverse N density vs. $p_\perp^{\text{clus1}}$	900 GeV		10
Transverse $\sum p_\perp$ density vs. $p_\perp^{\text{clus1}}$	900 GeV		10
Field & Stuart Run I underlying event analysis [33]			
N_{ch} (toward) for min-bias	1800 GeV	$\geq$ 4 GeV	3
N_{ch} (transverse) for min-bias	1800 GeV	$\geq$ 4 GeV	5
N_{ch} (away) for min-bias	1800 GeV	$\geq$ 4 GeV	3
N_{ch} (toward) for JET20	1800 GeV		3
N_{ch} (transverse) for JET20	1800 GeV		5
N_{ch} (away) for JET20	1800 GeV		3
$p_\perp^{\text{sum}}$ (toward) for min-bias	1800 GeV	$\geq$ 4 GeV	3
$p_\perp^{\text{sum}}$ (transverse) for min-bias	1800 GeV	$\geq$ 4 GeV	5
$p_\perp^{\text{sum}}$ (away) for min-bias	1800 GeV	$\geq$ 4 GeV	3

continued on next page

Observable	$\sqrt{s}$	Fit range	Weight
$p_\perp^{\text{sum}}$ (toward) for JET20	1800 GeV		3
$p_\perp^{\text{sum}}$ (transverse) for JET20	1800 GeV		5
$p_\perp^{\text{sum}}$ (away) for JET20	1800 GeV		3
$p_\perp$ distribution (transverse, $p_\perp^{\text{lead}} > 5$ GeV)	1800 GeV		3
$p_\perp$ distribution (transverse, $p_\perp^{\text{lead}} > 30$GeV)	1800 GeV		3
Transverse cone and 'Swiss cheese' underlying event studies [34]			
Transverse cone $\langle p_\perp^{\text{max}} \rangle$ vs. $E_\perp^{\text{lead}}$	1800 GeV		5
Transverse cone N_{max} vs. $E_\perp^{\text{lead}}$	1800 GeV		5
Swiss Cheese $p_\perp^{\text{sum}}$ vs. $E_\perp^{\text{lead}}$ (2 jets removed)	1800 GeV		5
Swiss Cheese $p_\perp^{\text{sum}}$ vs. $E_\perp^{\text{lead}}$ (3 jets removed)	1800 GeV		5
Transverse cone $\langle p_\perp^{\text{max}} \rangle$ vs. $E_\perp^{\text{lead}}$	630 GeV		5
Swiss Cheese $p_\perp^{\text{sum}}$ vs. $E_\perp^{\text{lead}}$ (2 jets removed)	630 GeV		5
Swiss Cheese $p_\perp^{\text{sum}}$ vs. $E_\perp^{\text{lead}}$ (3 jets removed)	630 GeV		5
CDF Run 2 underlying event in leading jet events [35]			
Transverse region charged particle density	1960 GeV		20
TransMAX region charged particle density	1960 GeV		10
TransMIN region charged particle density	1960 GeV		10
TransDIF region charged particle density	1960 GeV		2
Transverse region charged $\sum p_\perp$ density	1960 GeV		20
TransMAX region charged $\sum p_\perp$ density	1960 GeV		10
TransMIN region charged $\sum p_\perp$ density	1960 GeV		10
TransDIF region charged $\sum p_\perp$ density	1960 GeV		2
Transverse region charged $\langle p_\perp \rangle$ density	1960 GeV		10
CDF Run 2 underlying event in Drell-Yan [35]			
Toward region charged particle density	1960 GeV		20
Transverse region charged particle density	1960 GeV		10
TransMAX region charged particle density	1960 GeV		5
TransMIN region charged particle density	1960 GeV		5
Away region charged particle density	1960 GeV		5
Toward region charged $p_\perp^{\text{sum}}$ density	1960 GeV		20
Transverse region charged $p_\perp^{\text{sum}}$ density	1960 GeV		10
TransMAX region charged $p_\perp^{\text{sum}}$ density	1960 GeV		5
TransMIN region charged $p_\perp^{\text{sum}}$ density	1960 GeV		5
Away region charged $p_\perp^{\text{sum}}$ density	1960 GeV		5
Toward region charged $p_\perp^{\text{max}}$ density	1960 GeV		2
Transverse region charged $p_\perp^{\text{max}}$ density	1960 GeV		2
Away region charged $p_\perp^{\text{max}}$ density	1960 GeV		2
Charged $\langle p_\perp^{\ell\ell} \rangle$ vs. N_{ch}	1960 GeV		10
Charged $\langle p_\perp \rangle$ vs. N_{ch}	1960 GeV		10
Charged $\langle p_\perp \rangle$ vs. N_{ch}, $p_\perp(Z^0) < 10$ GeV	1960 GeV		10

Table 10: Observable–weight combinations used for the AUET2 MPI tuning. Where the fit has been made to a restricted range in leading $p_\perp$ or E_{T}, the fit range for that weight is shown in the "Fit range" column, expressed in GeV.

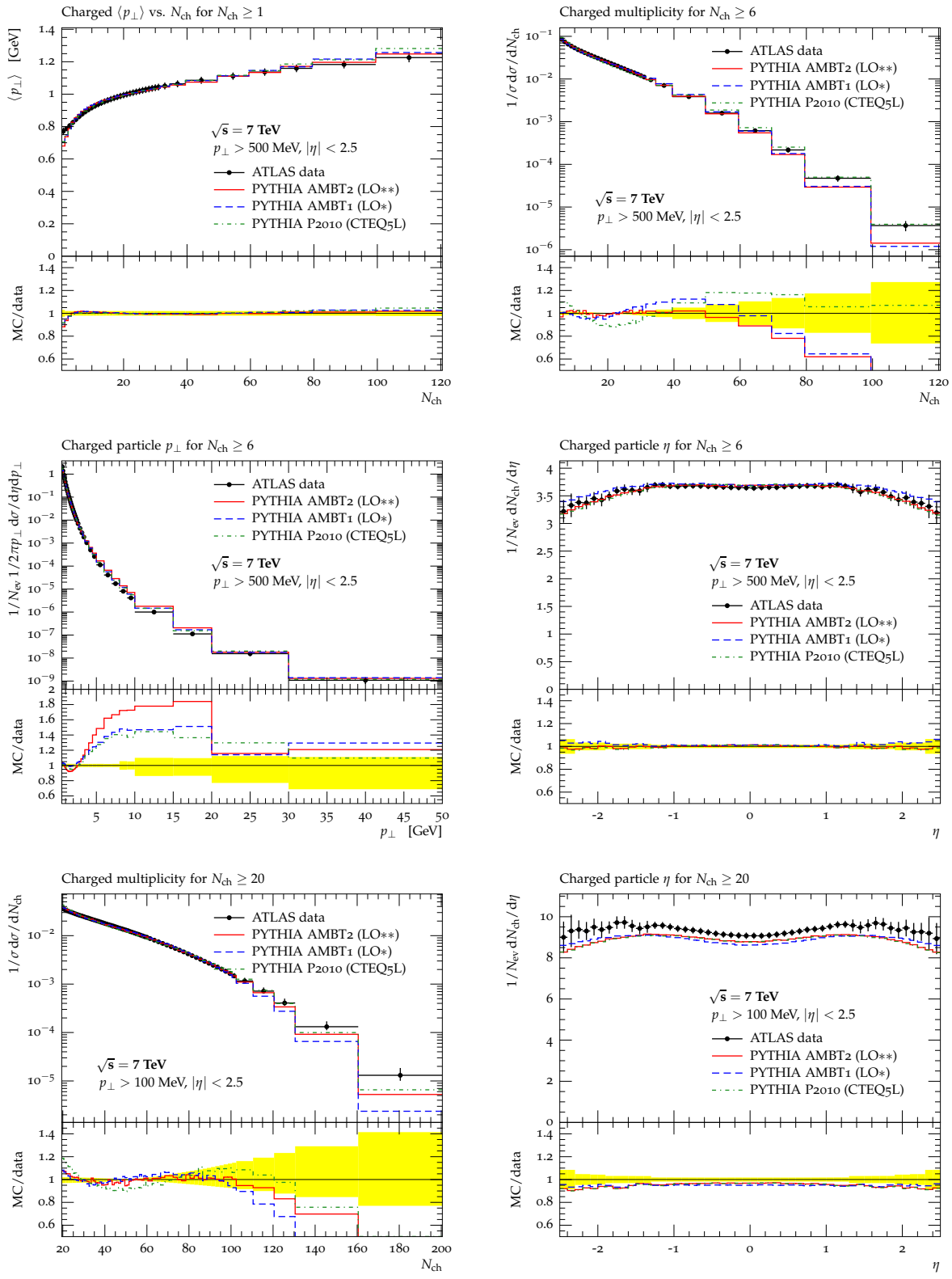

Figure 8: Comparison plots of the new Pythia 6 AMBT2 tune to ATLAS minimum bias data at 7 TeV. Unless explicitly stated, the track $p_\perp$ cut is 500 MeV.

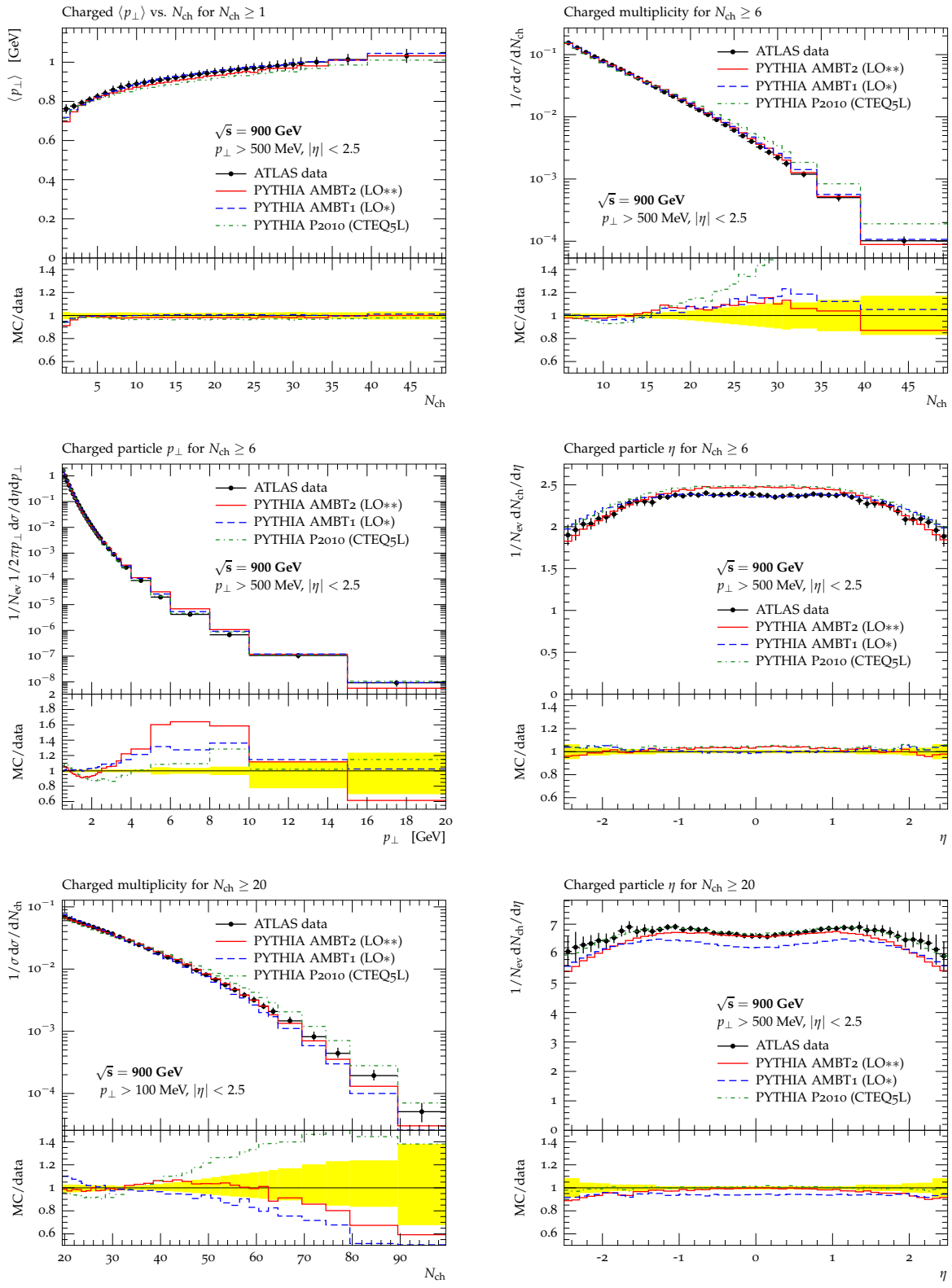

Figure 9: Comparison plots of the new Pythia 6 AMBT2 tune to ATLAS minimum bias data at 900 GeV. Unless explicitly stated, the track $p_\perp$ cut is 500 MeV.

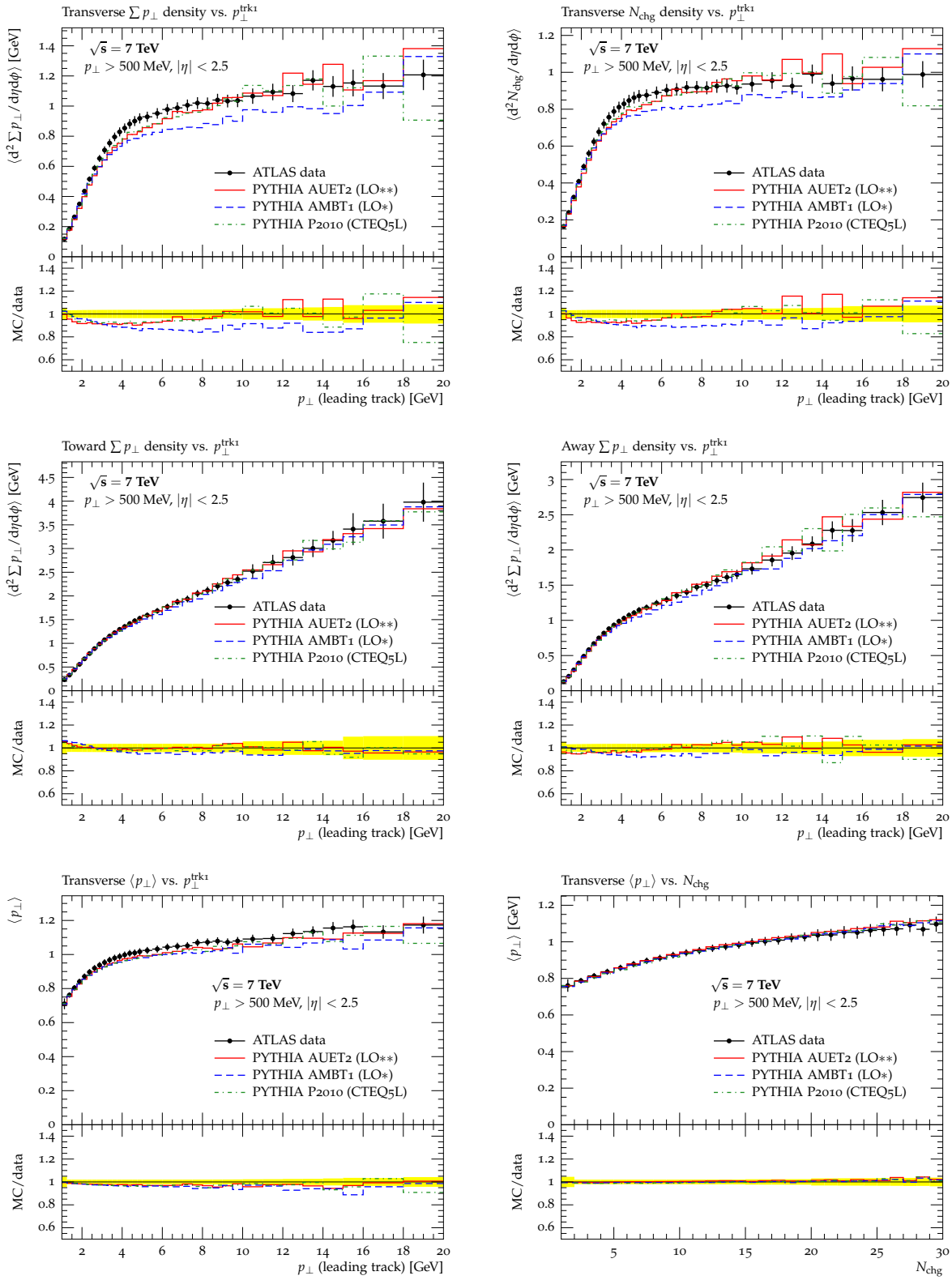

Figure 10: Comparison plots of the new Pythia 6 AUET2 tune to ATLAS underlying event data at 7 TeV. Unless explicitly stated, the track $p_\perp$ cut is 500 MeV.

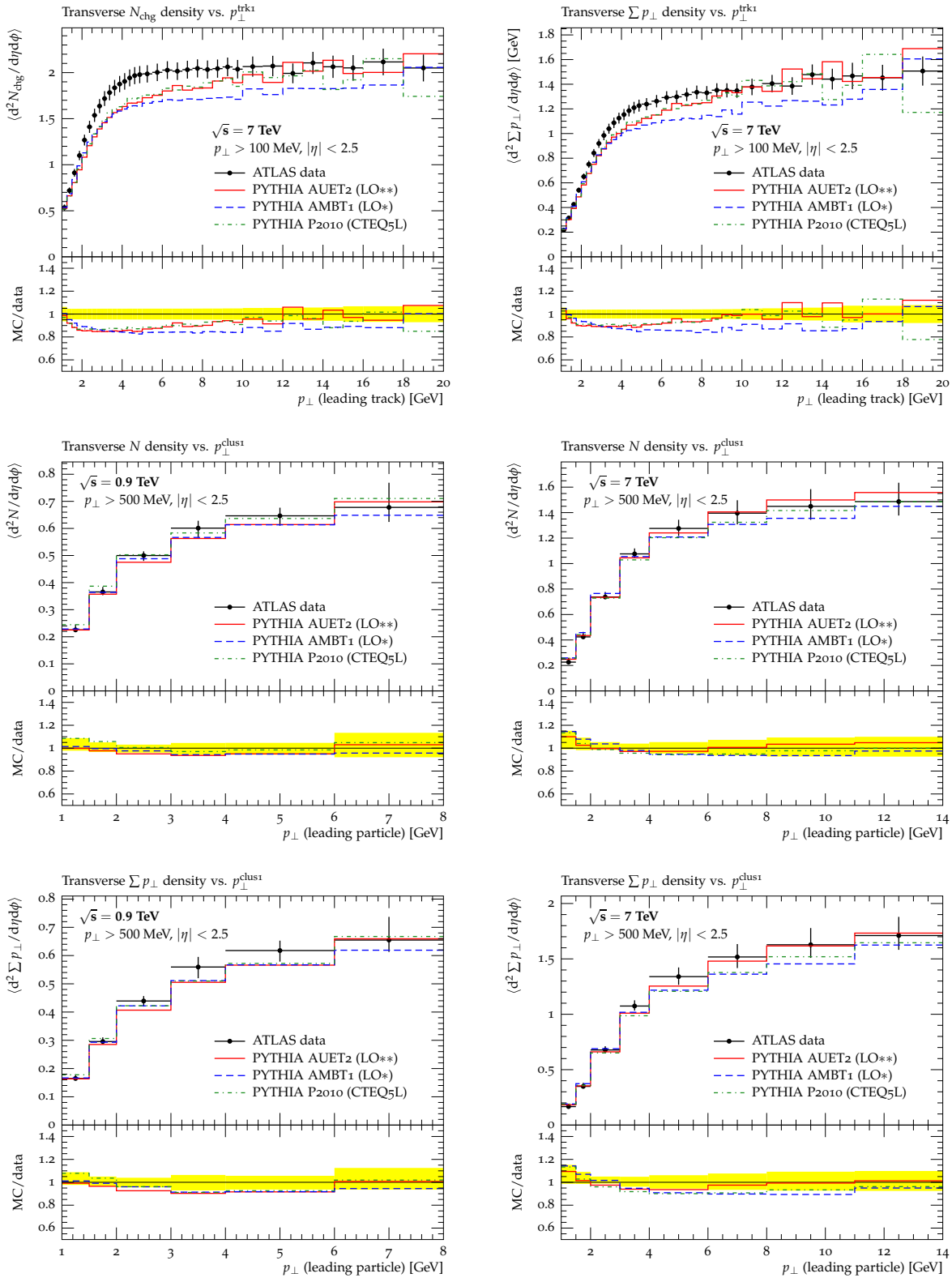

Figure 11: Comparison plots of the new Pythia 6 AUET2 tune to ATLAS underlying event data at 7 TeV. Unless explicitly stated, the track $p_{\perp}$ cut is 500 MeV.

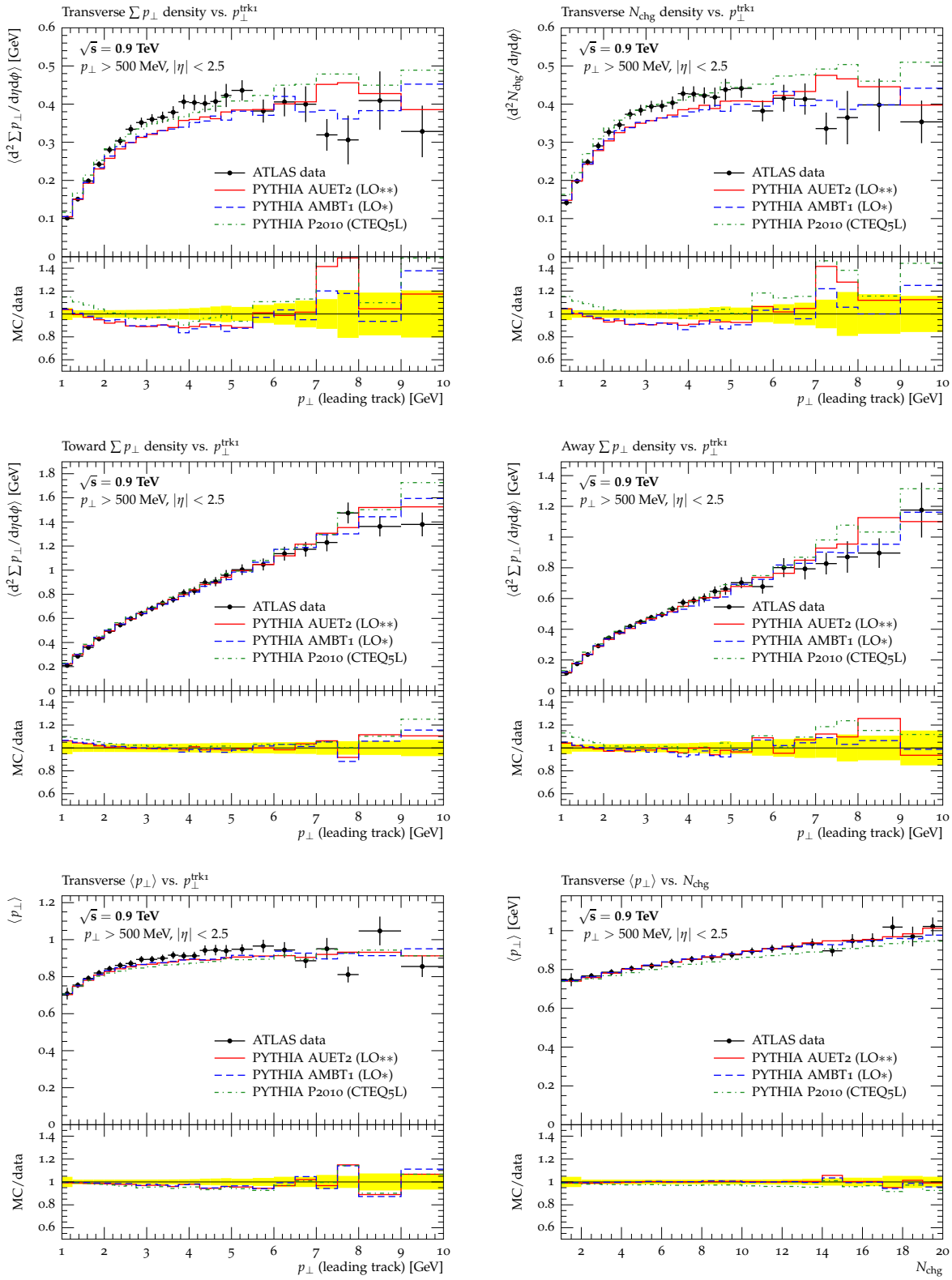

Figure 12: Comparison plots of the new Pythia 6 AUET2 tune to ATLAS underlying event data at 900 GeV. Unless explicitly stated, the track $p_\perp$ cut is 500 MeV.

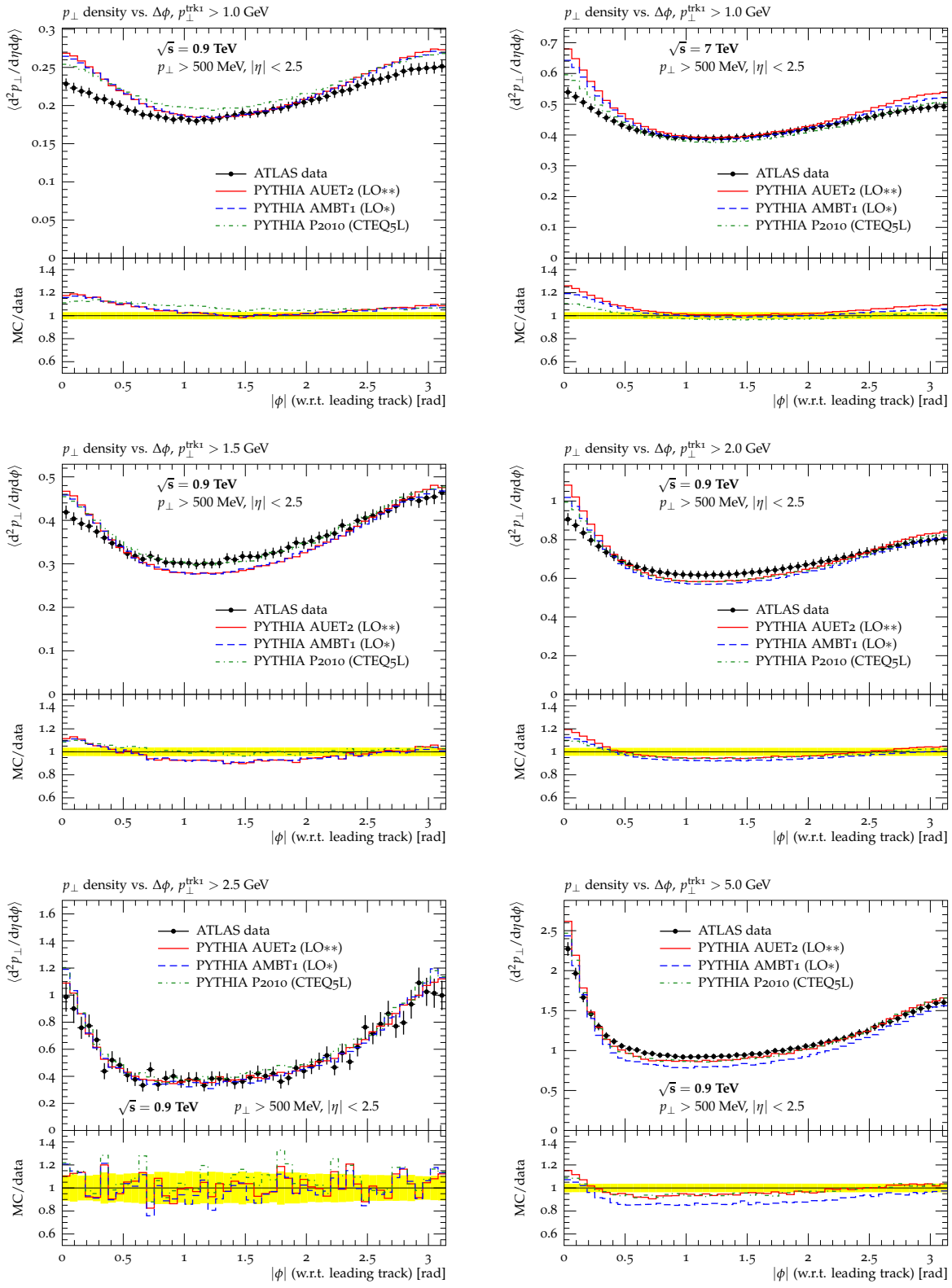

Figure 13: Comparison plots of the new Pythia 6 AUET2 tune to ATLAS underlying event data N_{ch} vs. $\Delta\phi$ at 900 GeV and 7 TeV, with a track $p_\perp$ cut of 500 MeV. These observables were not included in the tune.

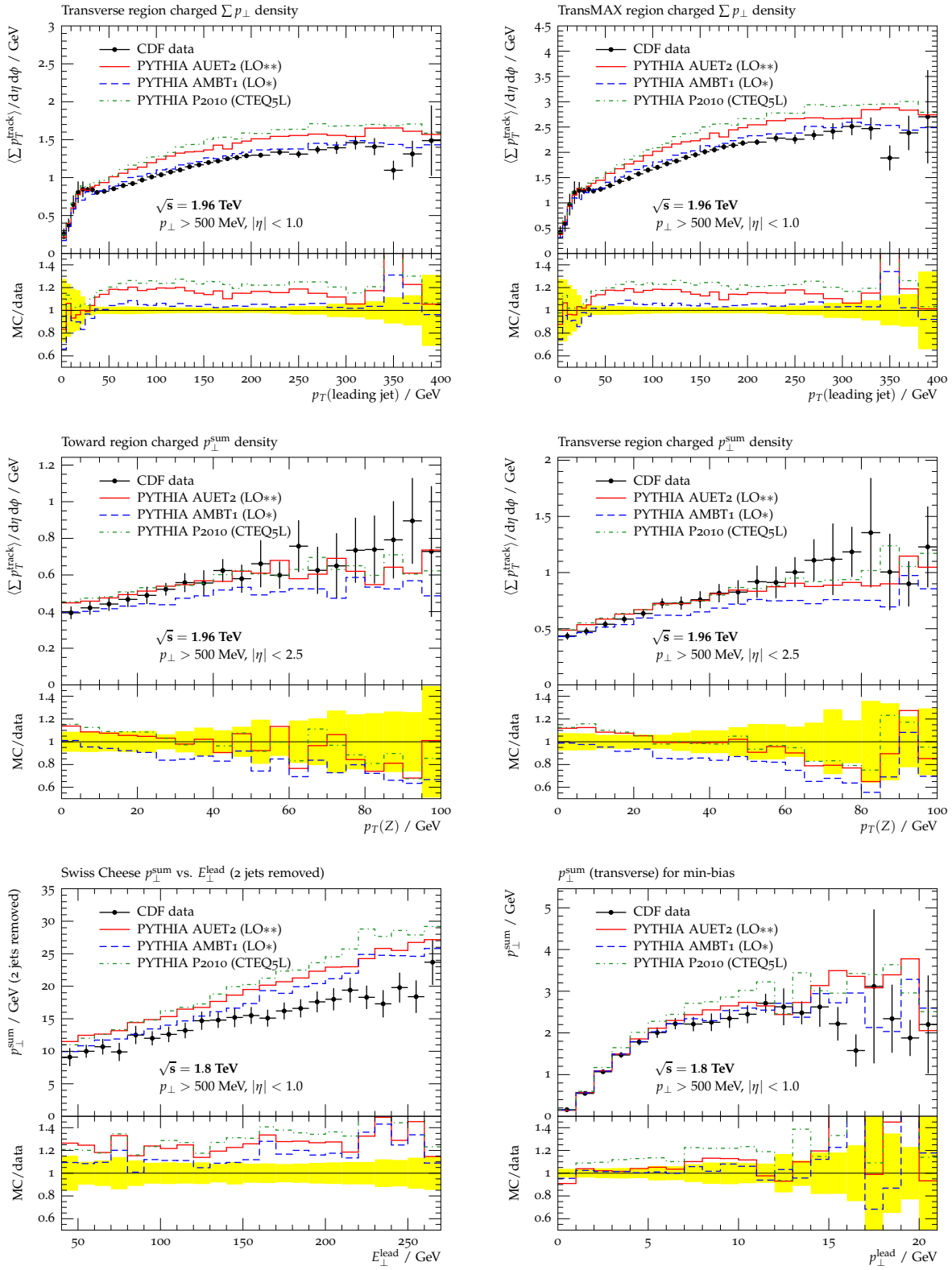

Figure 14: Comparison plots of the new Pythia 6 AUET2 tune to CDF underlying event data at 1800 and 1960 GeV.

2 Tuning of Herwig/Jimmy

The Herwig event generator is a general-purpose shower and hadronisation generator similar to Pythia 6 but with an angular-ordered (rather than $p_\perp$-ordered) parton showers, and a cluster-based rather than string-based hadronisation model. Notably, Herwig itself does not have an MPI model: this feature is added by the Jimmy add-on generator, and we refer to the combination in this note as Herwig/Jimmy. Both Herwig and Jimmy have fewer free parameters than are available in Pythia– in particular the initial and final state showers have few parameters – and so tuning is simpler than for Pythia. As with previous ATLAS tunes of Herwig/Jimmy, we concentrate here purely on the MPI parameters, all contained within Jimmy. As this is a single-stage tune, we have taken the opportunity to make equivalently-weighted tunes for ten different PDFs. We note here that the hadronisation parameters of Herwig have been left at the default values, i.e. untuned to LEP or other data, and so care must be taken in using Herwig/Jimmy as a reliable source of MC systematic uncertainties relating to hadronisation effects.

The Herwig/Jimmy tunes were, like that of Pythia 6, performed using the stand-alone AGILe 1.2.0 event generator interface to steer Herwig/Jimmy and to feed events to the Rivet 1.4.0 analysis package. For each tuning, several hundred points sampled from the Jimmy parameter space were used to construct parameterisations and hence optimised parameter sets via the Professor 1.2 MC tuning tool.

The generator setup is in all aspects the same as for MC10: one additional bug-fix release of Herwig was made after this tuning was well-progressed, and no update releases of Jimmy have been made since the MC10 tune preparations [1)].

Since the Jimmy MPI model is by design not valid for multiple scattering where the signal process is itself a soft scatter, minimum bias data cannot be used for tuning of this generator. As the underlying event data from ATLAS and CDF represent a smooth transition from minimum bias to UE-type processes, the softest parts of these observables must also be excluded from fits. In the ATLAS UE data, and that from the CDF 2001 UE study, the events are considered to be closer to minimum bias than hard QCD, and so Jimmy is instructed to generate the softest possible scatters by setting its UE mode to 0, via `JMUEO` $= 0$ and setting the lower phase space cut in p_{T}in hadronic jet production, `PTMIN`, to the value of the MPI cutoff, `PTJIM`.

2.1 Tuning parameters

The cut-off for multiple parton interactions modelled with Jimmy is a single parameter, `PTJIM`, without any dependence on $\sqrt{s}$. In order to make the model fit to data for various collider energies we apply the following energy dependence of `PTJIM` which is inspired by the "pomeron" energy evolution of the similar cut-off in the Pythia 6 model:

$$\texttt{PTJIM}(\sqrt{s}) = \texttt{PTJIM}_0 \cdot \left(\frac{\sqrt{s}}{1800\ \mathrm{GeV}} \right)^{\texttt{EXP}}, \tag{1}$$

where the tuning parameter $\texttt{PTJIM}_0$ is the value for `PTJIM` ($\sqrt{s}$) at the reference energy 1800 GeV. The energy exponent tuning parameter, `EXP`, was manually set at 0.274 in the MC08 Jimmy tune, and was kept fixed at this value in the MC09 Jimmy tunes (for all PDFs). The final MPI parameter for tuning is the hadronic form factor radius: although Jimmy allows the proton and antiproton radius to be set separately (`JMRAD(73)`, `JMRAD(93)`), we use the same variable, `PRRAD`, for both.

The relevant fixed settings and sampling ranges for these parameters, are shown in Table 11.

[1)] The AGILe interface to Herwig/Jimmy has received minor bug fixes and enhancements, all of which are minor.

Parameter i		i_{min}	i_{max}
Fixed parameters			
ISPAC	ISR-shower scheme	2	
PTRMS	Primordial $k_\perp$	1.2	
QSPAC	ISR shower cut-off	2.5	
Tuned cutoff meta-parameters			
PTJIM_0	MPI cut-off scale	1.5	5.5
EXP	MPI cut-off evolution	0.2	0.35
Tuned Jimmy parameters			
PRRAD	(Anti)proton radius	1.5	2.5

Table 11: Fixed parameter settings and sampling boundaries for tuned (meta-) parameters $i_{\text{min/max}}$. The settings were the same for the 10 tunings for different PDFs.

PDF type	PDF set	LHAPDF code	N_{runs}	$N_{\text{runs}}/N_{\text{min}}$
Leading order (LO)	CTEQ6L1 [36]	10042	77	3.85
	MSTW08LO [37]	21000	85	4.25
Modified leading order (mLO)	MRSTMCal (LO**) [16]	20651	59	2.95
	CT09MC2 [38]	10772	56	2.80
Next-to leading order (NLO)	CTEQ6.6 [39]	10550	78	3.90
	CT10 [40]	10800	83	4.15
	MSTW08NLO [37]	21100	82	4.10
	HERAPDF1.0 [41]	60500	68	3.40
	HERAdis [42]	USERGRID [a)]	52	2.60
	NNPDF2.1 [43]	192800	68	3.40

[a)] This PDF set is not a standard member of LHAPDF but can be used via the USERGRID interface.

Table 12: PDF sets used for tuning, available MC generator runs and degree of oversampling, $N_{\text{runs}}/N_{\text{min}}$

2.2 PDF sets

The AUET1 tunings of Jimmy/Herwig consisted of tuning the same generator setup to three different PDFs. The result of which already suggested that the PDF-effect can be absorbed by the MPI-parameters almost completely. For the AUET2 tunings the tuning was repeated for a total of ten PDFs, among which are leading order, modified leading order and next-to leading order PDFs from different PDF groups such as CTEQ, MSTW and, for the first time, also HERA and NNPDF2.1. The PDFs used in the tunings and the corresponding LHAPDF-codes as well as the total number of successful MC generator runs available as input for the Professor parameterisations are given in Table 12.

2.3 Observable selection

The model has been stretched with the previous AUET1 [5] tunes already, given e.g. the need to introduce an energy-dependence of the MPI cutoff, the missing soft physics and the observed inability of the model to describe $\sum p_\perp$ and N_{ch} observables equally well.

In this tuning round it was observed that the ansatz in Eq. (1) is *not* suited to fit the model to data from more than two energies (we consider 1.8 TeV and 1.96 TeV as on energy point). Thus we had to drop the available 630 GeV data from CDF and the 900 GeV data from ATLAS, such that the tuning input comes from 7 TeV and ~ 2 TeV data only.

The most striking difference to AUET1 besides the exclusion of the low energy data is the use of the high statistics version of the ATLAS track-based UE analysis, the use of the recently published ATLAS topocluster UE analysis, (which in contrast to the track-based analysis also accounts for neutral particles) as well as the addition of the recently published UE analyses from CDF Run 2 using both jet and Drell-Yan events [35].

The weights on the $\sum p_\perp$ observables have been set higher than those for the N_{ch} ones, although this time the weights are not as imbalanced as they were in AUET1.

The input to the Professor minimisation stage has been developed using the parametrisation built from the MC histograms generated with the LO** PDF and were applied in the tunings using the other PDFs unchanged. Care has been taken to exclude the aforementioned parts of distributions governed by soft physics. The complete listing of those observable/weight combinations used for all tunings can be found in Table 15.

2.4 Tuning results

We tuned Jimmy/Herwig using ten different PDFs and found that the data distributions can be described to a similar degree for all PDFs. The Figures 16–22 show these tunes, and are organised as follows: for each observable there are two plots per row, of which the left-hand plot shows the comparison of data to the AUET2 tunes for the LO and mLO PDFs, as well as the AUET1 tune for the mLO LO* PDF; the right-hand plot is a comparison of data with all the AUET2 tunes for NLO PDFs. The selection of observables includes UE distributions from ATLAS and CDF Run II.

Given that the focus has clearly been on the ATLAS 7 TeV and CDF Run II data it is not surprising that those distributions are described best. We find an equally good reproduction of the 7 TeV data for charged and charged and neutral particles. Note that in all UE profiles in the leading jet or charged particle $p_\perp$, the Jimmy MPI mechanism deviates significantly from the data at low $p_\perp$: this is an expected model feature and does not herald a problem with the tuning, as Jimmy is not intended to describe inclusive MPI in this minimum bias region.

The global description of the $\sum p_\perp$ observables is better than that of their N_{ch} counterparts, as slightly more fit weight was placed on the $p_\perp$ observables. The Jimmy/Herwig model does not have as many parameters as in Pythia 6, where a "colour reconnection" mechanism can be used to level out the differences between the two classes of observable, and so one will always be described better than the other. This is particularly obvious in the observables featuring $\langle p_\perp \rangle$. Furthermore it was observed that the available parameters are very well able to shift the UE profiles up and down but fail to influence the shapes significantly. The regions governed by soft physics aren't described due to the missing soft physics in Jimmy/Herwig.

Given that the tuned parameter value for the inverse proton radius, `PRRAD`, is significantly higher in AUET2 than in AUET1, a further shortcoming of the model could be a non-trivial and so far unaccounted energy dependence of this parameter, too.

It can generally be said that the PDF effect can be "tuned away" with the available parameters, meaning that very similar agreement can be reached for all PDFs studied. However some differences are visible, e.g. the $\langle p_\perp \rangle$ vs. N_{ch} observables are a bit better described by the mLO PDFs than by the LO and NLO PDFs.

Another finding is that the ATLAS distributions with the lowered track $p_\perp$ cut of 100 MeV are not possible

to describe, Herwig/Jimmy produces too many too hard particles. This is very likely due to the missing soft physics in the model.

Grouping of tuned parameters by PDF

We observed that the obtained tuning results for the cutoff parameter PTJIM group according to the PDF type with the mLO PDFs yielding the highest values, followed by the LO and the NLO PDFs. Since a high cutoff values means that less activity is required by the parton shower to match the data this result is in agreement with the expectation that the mLO PDFs create more activity from the beginning.

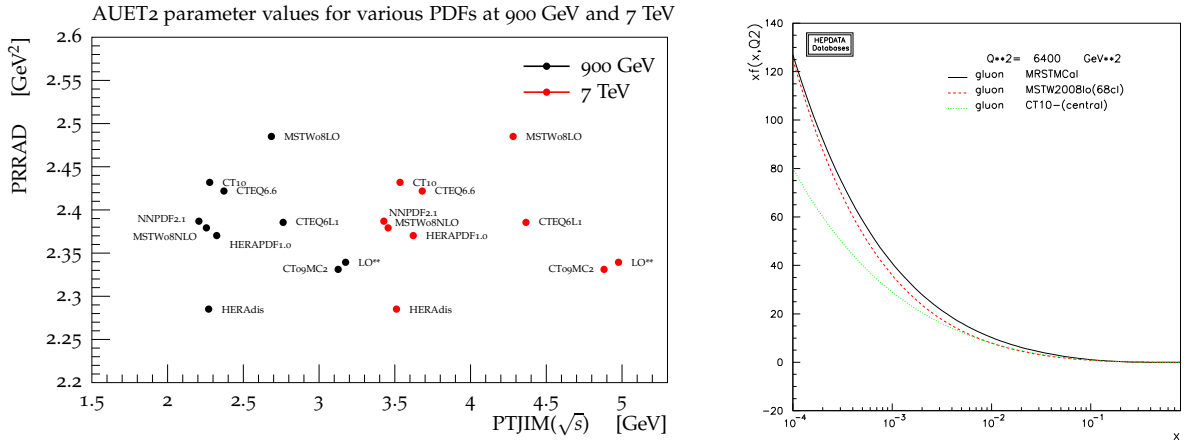

Figure 15: (a) Observed grouping of tuning results of PTJIM by PDF type. The corresponding numbers are given in Tables 13 and 14. (b) Gluon density distributions ($Q^2 = 6400$ GeV^2) for LO (MSTW08LO), mLO (MRSTCAL, LO**) and NLO (CT10) PDFs, illustrating the augmented gluon activity at low x for mLO PDFs (plot generated at `http://hepdata.cedar.ac.uk/pdfs`)

PDF set	CTEQ6L1	MSTW08LO	CT09MC2	LO**
PRRAD	2.386	2.485	2.331	2.339
PTJIM_0	3.224	3.424	3.634	3.696
EXP	0.231	0.227	0.217	0.219
PTJIM (900 GeV)	2.747	2.925	3.127	3.175
PTJIM (2760 GeV)	3.559	3.773	3.987	4.059
PTJIM (7000 GeV)	4.412	4.660	4.880	4.976

Table 13: Final tuning results for LO and mLO PDFs

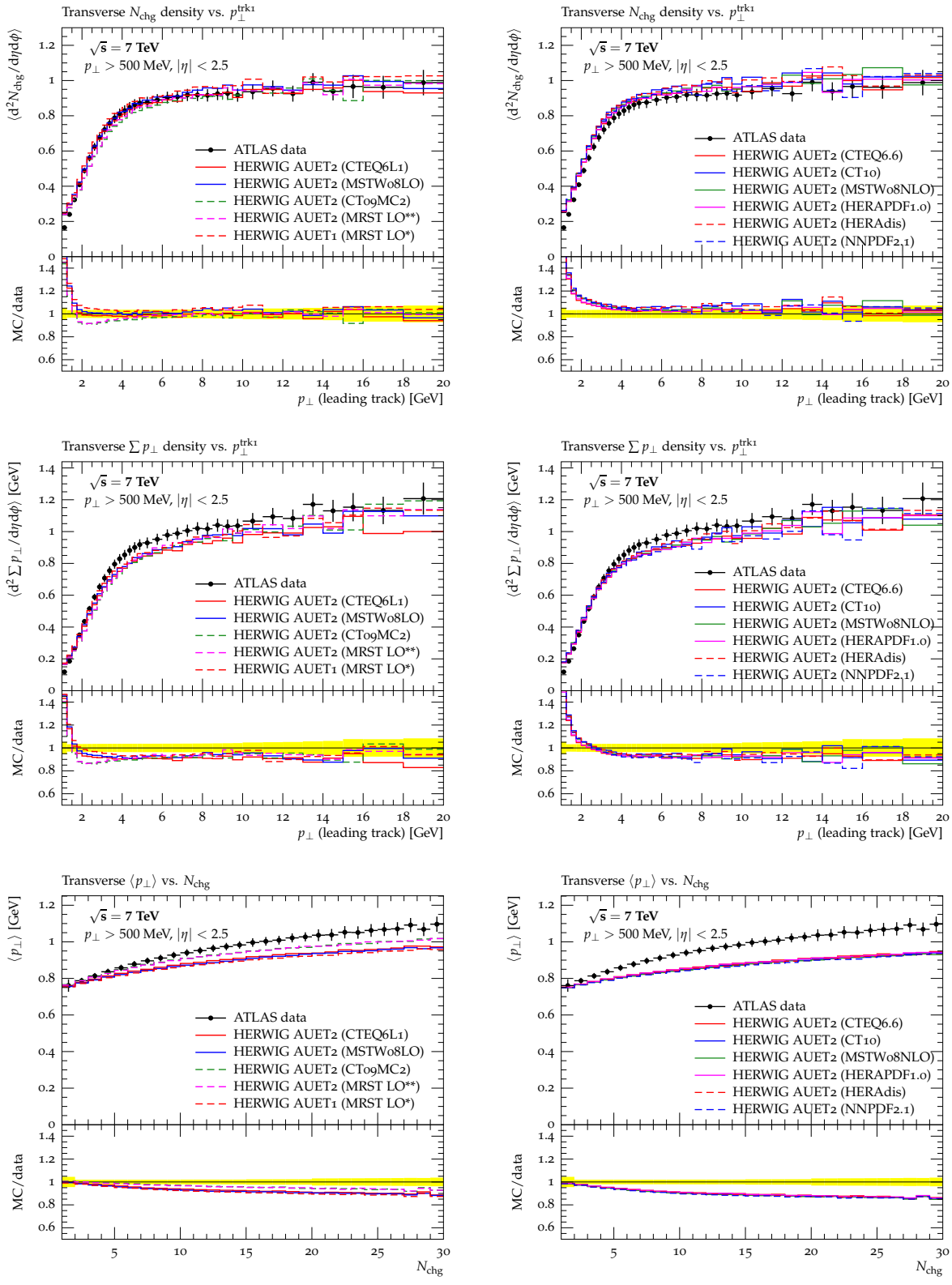

Figure 16: Comparison plots of the new Herwig/Jimmy AUET2 tunes to 7 TeV ATLAS track-based UE data. Left column: LO and mLO PDFs. Right column: NLO PDFs. The track $p_{\perp}$ cut for all observables is 500 MeV.

PDF set	CTEQ6.6	MSTW08NLO	HERAPDF1.0	HERAdis	CT10	NNPDF2.1
PRRAD	2.422	2.387	2.370	2.285	2.432	2.387
$\texttt{PTJIM}_0$	2.752	2.606	2.700	2.631	2.642	2.561
EXP	0.214	0.208	0.216	0.212	0.214	0.215
PTJIM (900 GeV)	2.373	2.256	2.325	2.271	2.278	2.206
PTJIM (2760 GeV)	3.016	2.848	2.961	2.881	2.895	2.808
PTJIM (7000 GeV)	3.680	3.457	3.620	3.509	3.533	3.429

Table 14: Final tuning results for NLO PDFs

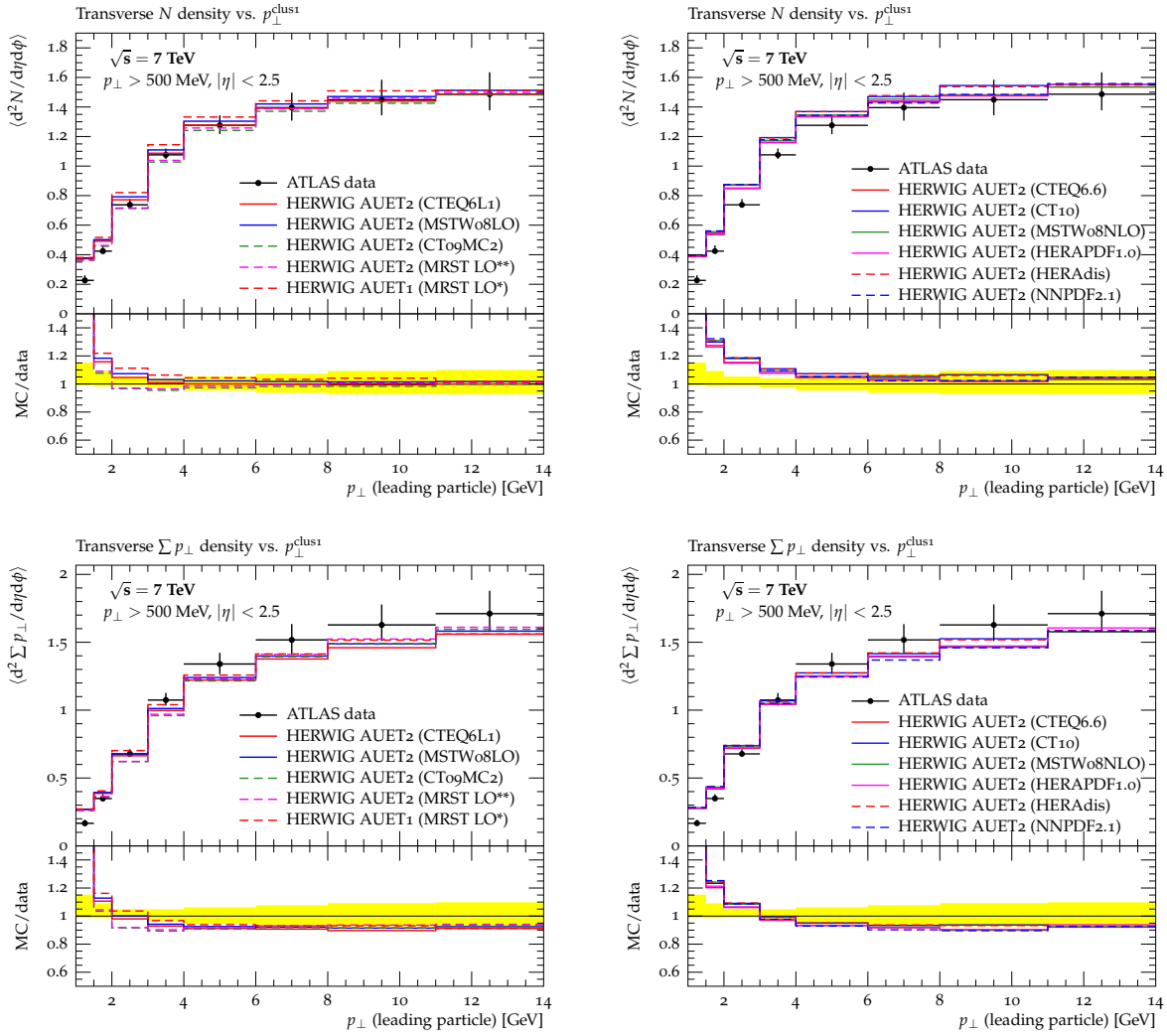

Figure 17: Comparison plots of the new Herwig/Jimmy AUET2 tunes to 7 TeV ATLAS cluster-based UE data. Left column: LO and mLO PDFs. Right column: NLO PDFs. The track $p_\perp$ cut for all observables is 500 MeV.

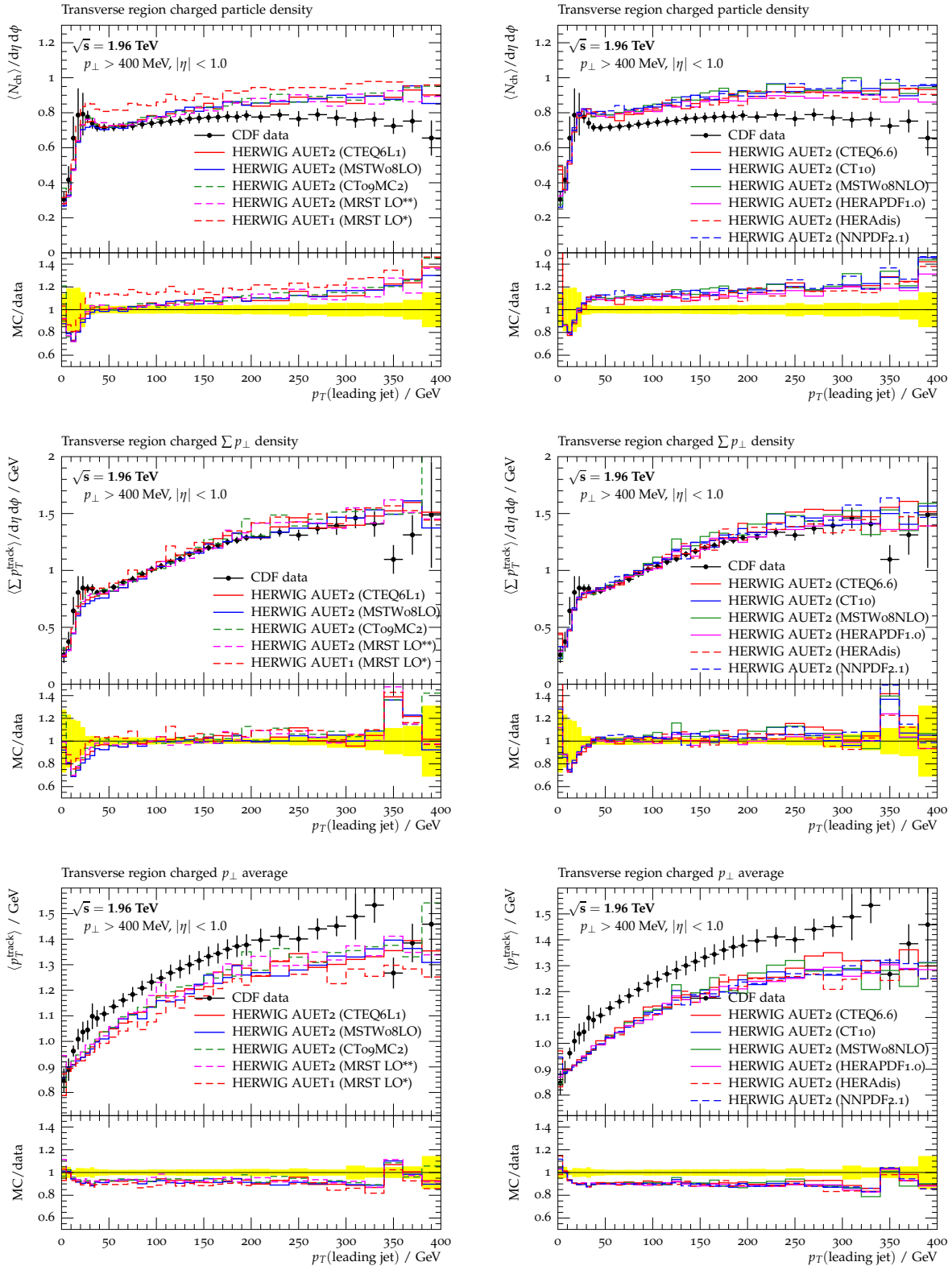

Figure 18: Comparison plots of the new Herwig/Jimmy AUET2 tunes to CDF Run II leading jet data at 1.96 TeV. Left column: LO and mLO PDFs. Right column: NLO PDFs.

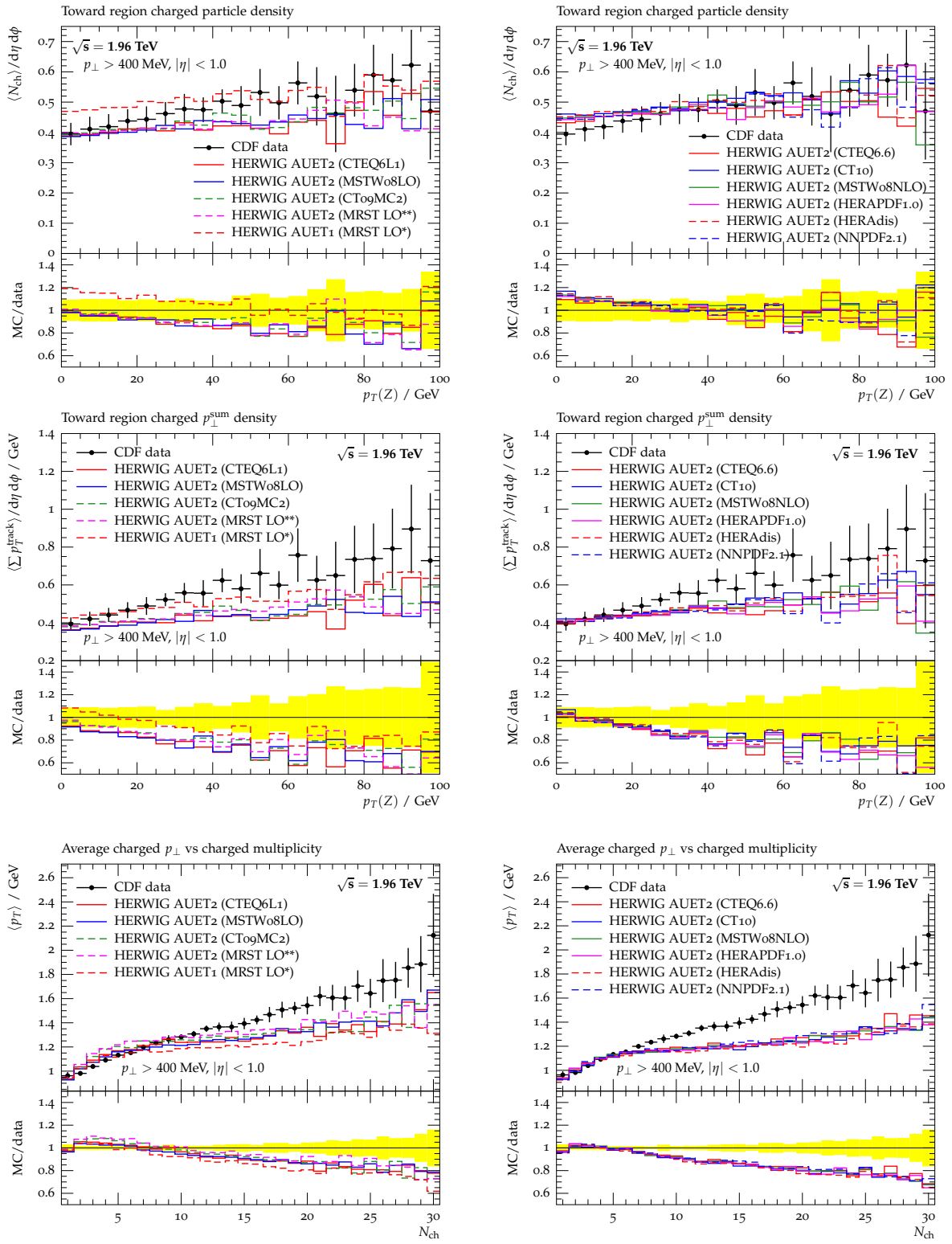

Figure 19: Comparison plots of the new Herwig/Jimmy AUET2 tunes to CDF Run II Drell-Yan data at 1.96 TeV. Left column: LO and mLO PDFs. Right column: NLO PDFs.

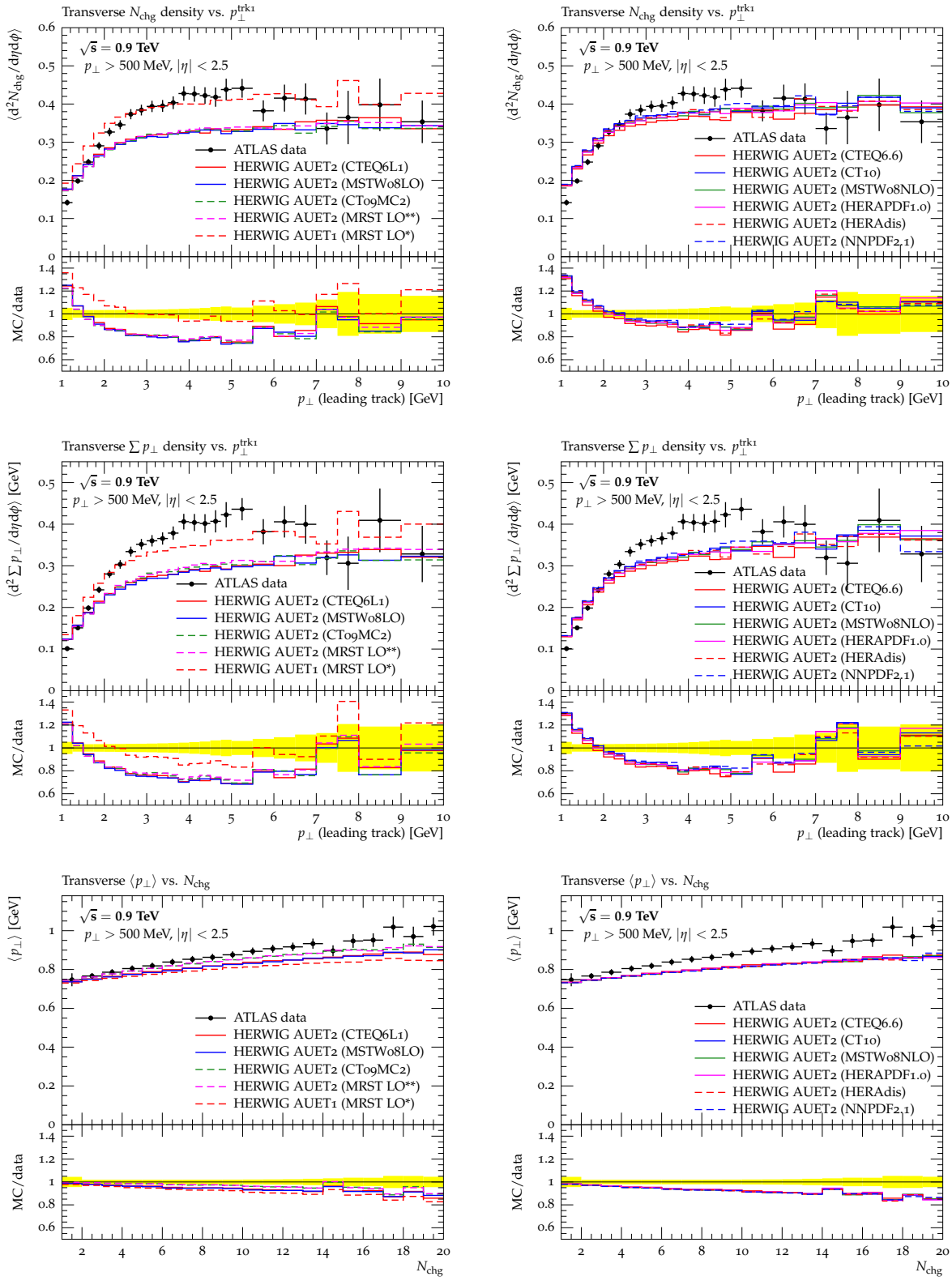

Figure 20: Comparison plots of the new Herwig/Jimmy AUET2 tunes to 900 GeV ATLAS track-based UE data. Left column: LO and mLO PDFs. Right column: NLO PDFs. The track $p_{\perp}$ cut for all observables is 500 MeV.

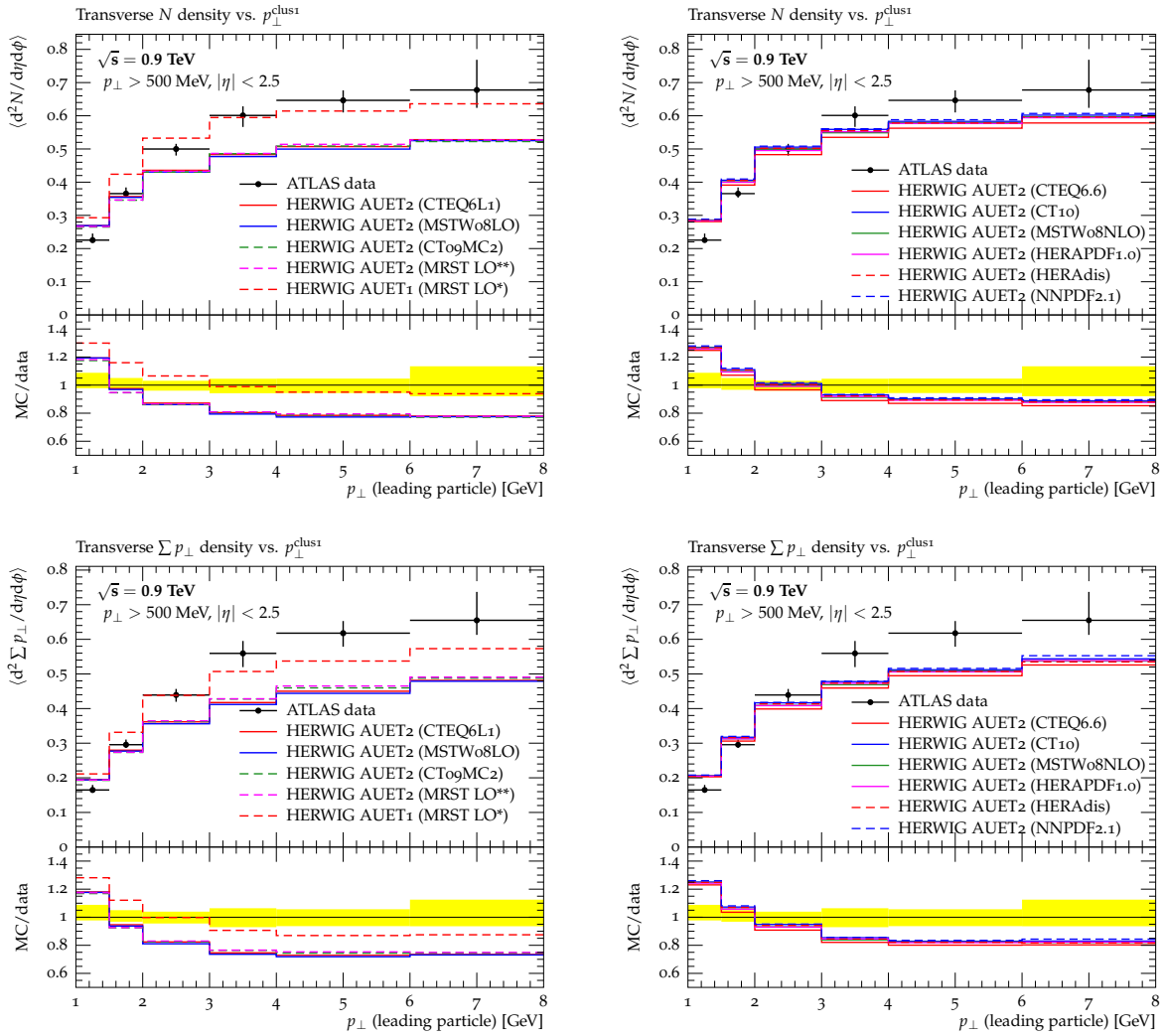

Figure 21: Comparison plots of the new Herwig/Jimmy AUET2 tunes to 900 GeV ATLAS cluster-based UE data. Left column: LO and mLO PDFs. Right column: NLO PDFs. The track $p_{\perp}$ cut for all observables is 500 MeV.

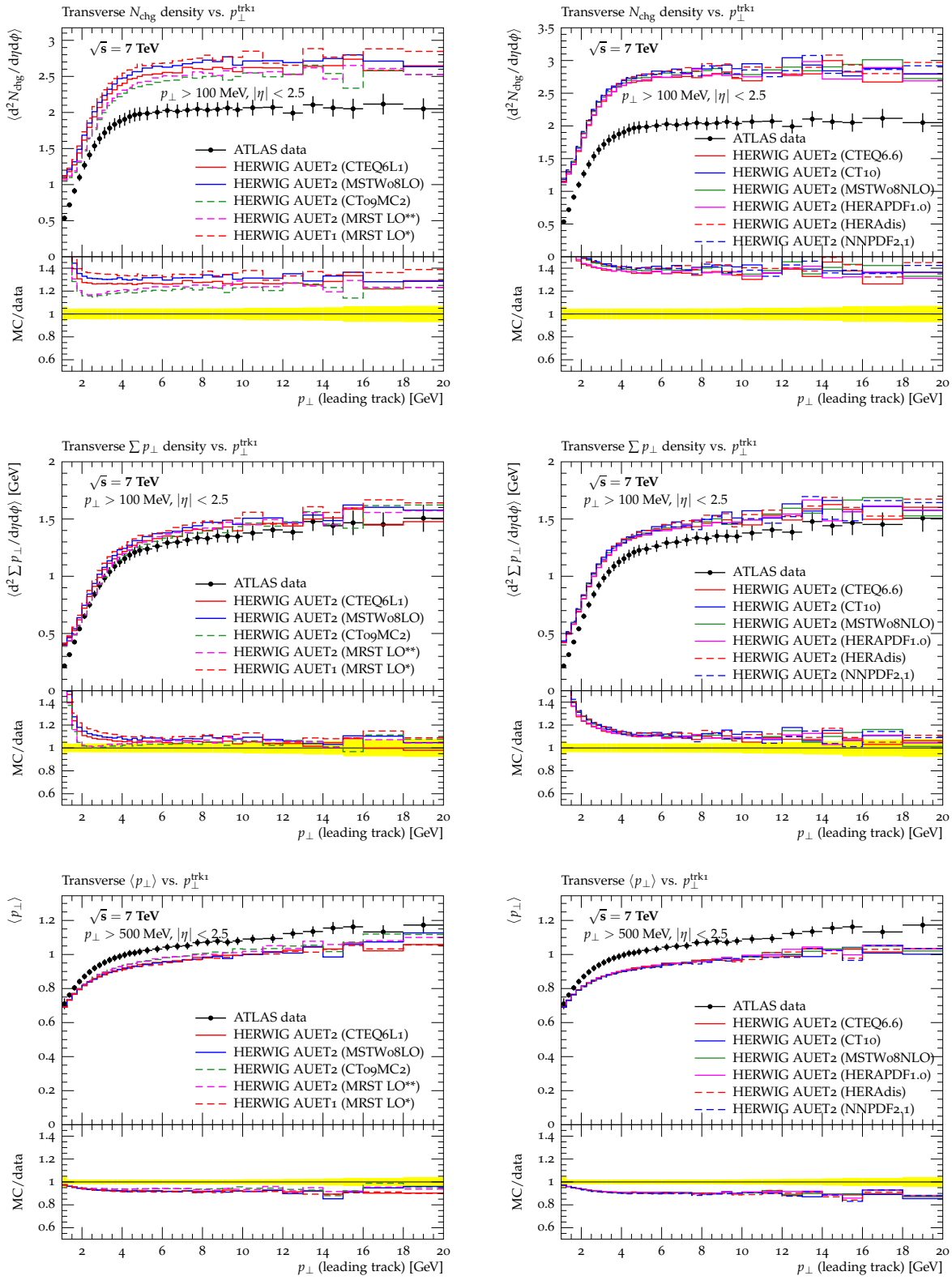

Figure 22: Comparison plots of the new Herwig/Jimmy AUET2 tunes to 7 TeV ATLAS data. Left column: LO and mLO PDFs. Right column: NLO PDFs.

Observable	$\sqrt{s}$	Fit range	Weight	JMUEO	PTMIN
Track-based underlying event at 900 GeV and 7 TeV in ATLAS [2]					
Transverse region N_{chg} density vs. $p_\perp$ (leading track)	7 TeV	$\geq$ 6 GeV	40	0	PTJIM
Toward region N_{chg} density vs. $p_\perp$ (leading track)	7 TeV	$\geq$ 6 GeV	10	0	PTJIM
Away region N_{chg} density vs. $p_\perp$ (leading track)	7 TeV	$\geq$ 6 GeV	10	0	PTJIM
Transverse region $\sum p_\perp$ density vs. $p_\perp$ (leading track)	7 TeV	$\geq$ 6 GeV	60	0	PTJIM
Toward region $\sum p_\perp$ density vs. $p_\perp$ (leading track)	7 TeV	$\geq$ 6 GeV	10	0	PTJIM
Away region $\sum p_\perp$ density vs. $p_\perp$ (leading track)	7 TeV	$\geq$ 6 GeV	10	0	PTJIM
Transverse N density vs. $p_\perp^{\text{clus1}}$	7 TeV	$\geq$ 4 GeV	50	0	PTJIM
Transverse $\sum p_\perp$ density vs. $p_\perp^{\text{clus1}}$	7 TeV	$\geq$ 6 GeV	100	0	PTJIM
Cluster-based underlying event at 900 GeV and 7 TeV in ATLAS [3]					
Transverse N density vs. $p_\perp^{\text{clus1}}$	7 TeV	$\geq$ 4 GeV	50	0	PTJIM
Transverse $\sum p_\perp$ density vs. $p_\perp^{\text{clus1}}$	7 TeV	$\geq$ 6 GeV	100	0	PTJIM
Field & Stuart Run I underlying event analysis [33]					
N_{ch} (toward) for min-bias	1800 GeV	$\geq$ 4 GeV	1	0	PTJIM
N_{ch} (transverse) for min-bias	1800 GeV	$\geq$ 4 GeV	1	0	PTJIM
N_{ch} (away) for min-bias	1800 GeV	$\geq$ 4 GeV	1	0	PTJIM
N_{ch} (toward) for JET20	1800 GeV		1	1	10 GeV
N_{ch} (transverse) for JET20	1800 GeV		2	1	10 GeV
N_{ch} (away) for JET20	1800 GeV		1	1	10 GeV
$p_\perp^{\text{sum}}$ (toward) for min-bias	1800 GeV	$\geq$ 4 GeV	1	0	PTJIM
$p_\perp^{\text{sum}}$ (transverse) for min-bias	1800 GeV	$\geq$ 4 GeV	1	0	PTJIM
$p_\perp^{\text{sum}}$ (away) for min-bias	1800 GeV	$\geq$ 4 GeV	1	0	PTJIM
$p_\perp^{\text{sum}}$ (toward) for JET20	1800 GeV		1	1	10 GeV
$p_\perp^{\text{sum}}$ (transverse) for JET20	1800 GeV		2	1	10 GeV
$p_\perp^{\text{sum}}$ (away) for JET20	1800 GeV		1	1	10 GeV
$p_\perp$ distribution (transverse, $p_\perp^{\text{lead}} > 5$ GeV)	1800 GeV		1	1	10 GeV
$p_\perp$ distribution (transverse, $p_\perp^{\text{lead}} > 30$GeV)	1800 GeV		1	1	10 GeV
Transverse cone and 'Swiss cheese' underlying event studies [34]					
Transverse cone $\langle p_\perp^{\text{max}} \rangle$ vs. $E_\perp^{\text{lead}}$	1800 GeV		1	1	10 GeV
Transverse cone N_{max} vs. $E_\perp^{\text{lead}}$	1800 GeV		1	1	10 GeV
Swiss Cheese $p_\perp^{\text{sum}}$ vs. $E_\perp^{\text{lead}}$ (2 jets removed)	1800 GeV		1	1	10 GeV
Swiss Cheese $p_\perp^{\text{sum}}$ vs. $E_\perp^{\text{lead}}$ (3 jets removed)	1800 GeV		1	1	10 GeV
CDF Run 2 underlying event in leading jet events [35]					
Transverse region charged particle density	1960 GeV	$30 \leq x \leq 300$ GeV	3	1	10 GeV
TransMAX region charged particle density	1960 GeV	$30 \leq x \leq 300$ GeV	1	1	10 GeV
TransMIN region charged particle density	1960 GeV	$30 \leq x \leq 300$ GeV	1	1	10 GeV
TransDIF region charged particle density	1960 GeV	$30 \leq x \leq 300$ GeV	1	1	10 GeV
Transverse region charged $\sum p_\perp$ density	1960 GeV	$30 \leq x \leq 300$ GeV	6	1	10 GeV
TransMAX region charged $\sum p_\perp$ density	1960 GeV	$30 \leq x \leq 300$ GeV	2	1	10 GeV
TransMIN region charged $\sum p_\perp$ density	1960 GeV	$30 \leq x \leq 300$ GeV	2	1	10 GeV
TransDIF region charged $\sum p_\perp$ density	1960 GeV	$30 \leq x \leq 300$ GeV	2	1	10 GeV
CDF Run 2 underlying event in Drell-Yan [35]					
Toward region charged particle density	1960 GeV	$\geq$ 10 GeV	2	1	10 GeV
Transverse region charged particle density	1960 GeV	$\geq$ 10 GeV	1	1	10 GeV
TransMAX region charged particle density	1960 GeV	$\geq$ 10 GeV	1	1	10 GeV
TransMIN region charged particle density	1960 GeV	$\geq$ 10 GeV	1	1	10 GeV
TransDIF region charged particle density	1960 GeV	$\geq$ 10 GeV	1	1	10 GeV
Away region charged particle density	1960 GeV	$\geq$ 10 GeV	1	1	10 GeV
Toward region charged $p_\perp^{\text{sum}}$ density	1960 GeV	$\geq$ 10 GeV	4	1	10 GeV
Transverse region charged $p_\perp^{\text{sum}}$ density	1960 GeV	$\geq$ 10 GeV	2	1	10 GeV
TransMAX region charged $p_\perp^{\text{sum}}$ density	1960 GeV	$\geq$ 10 GeV	2	1	10 GeV

continued on next page

Observable	$\sqrt{s}$	Fit range	Weight	JMUEO	PTMIN
TransMIN region charged $p_\perp^{\text{sum}}$ density	1960 GeV	$\geq$ 10 GeV	2	1	10 GeV
TransDIF region charged $p_\perp^{\text{sum}}$ density	1960 GeV	$\geq$ 10 GeV	2	1	10 GeV
Away region charged $p_\perp^{\text{sum}}$ density	1960 GeV	$\geq$ 10 GeV	2	1	10 GeV

Table 15: Observable–weight combinations used for the final tunings. Where the fit has been made to a restricted range in leading $p_\perp$ or E_{T}, the fit range for that weight is shown in the "Fit range" column, expressed in GeV.

3 Conclusions

We have presented new tunes of the Pythia 6 and Herwig/Jimmy event generators, based on the maximum available ATLAS data from the 2010 data taking period. The Pythia tune is based on the setup of the Perugia 2010 tune and is a full-chain tune including hadronisation and the final state parton shower, the initial state parton shower, and the multiple-parton interactions mechanism, using the LO** PDF. The Herwig/Jimmy tunes are MPI-only, but are constructed for a total of 10 PDFs, including LO, NLO, and mLO types both old and new – note that the Herwig shower and hadronisation models remain untuned and should be treated with care in physics analyses.

The Pythia tuning was motivated largely by the desire to improve the description of jet shape observables, and this was achieved, as in the Perugia 2010 tune, by using a more FSR-like definition of Λ_{QCD} for the evaluation of α_S in final state showering from ISR partons. Several other jet-related quantities have also improved as a result of this tuning. The MPI tuning makes use of the full-statistics forms of the ATLAS minimum bias and underlying event analyses at 900 GeV and 7 TeV, including the recently published cluster UE analysis. The treatment of Λ_{QCD} in both new tunes was found to have several pitfalls including an up-scaling of the effective value by a factor of ~ 1.6 in the ISR, and that the Λ_{QCD} base values used in other tunes were not in fact based on those in the PDFs, which caused sampling range problems in the MPI tuning.

These factors may be responsible for changes in ISR behaviour from the MC09/AMBT1 experience: simultaneous fitting of MB and UE observables was found to be impossible, leading to a *pair* of tunes, AMBT2 and AUET2, and the description of UE profile shapes and minimum bias $p_\perp$ spectra was also found to be beyond the scope of the MPI parametrisation given our ISR/FSR configuration. The worsening of the minimum bias $p_\perp$ spectrum description by AMBT2 by comparison to AMBT1 is likely to be due to the changes in shower modelling. This does not rule out use of AMBT2 for minimum bias studies – there are improvements over AMBT1 in several other observables, including the statistically dominant part of the N_{ch} distribution – but it is perhaps better considered as a systematic partner of AMBT1 rather than a replacement. The Pythia AUET2 tune is more definitively an improvement over AMBT1 for underlying event and signal process simulation.

The Herwig/Jimmy tuning was more straightforward, having fewer parameters and relevant observables than for Pythia, and it demonstrates the degree to which MC tuning can be "industrialised" to construct equivalent tunes for many PDFs. It has been observed that a very similar description of UE data can be achieved regardless of the PDF type. Moreover we find that the obtained tuning results group according to the PDF type in the MPI cutoff scale parameter, PTJIM. These tunes also display the limitations of the Jimmy MPI model: we find that the energy evolution ansatz for the MPI cutoff in Eq. (1) is not sufficient to describe data at all energies available: more precisely, a good description of data is only possible when not more than two energies are considered in the fit. We therefore decided to drop the low energy data from ATLAS and CDF to be able to get a good reproduction of the Run II UE data from CDF which is more important for the LHC programme given the 2011 run at $\sqrt{s} = 2.76$ TeV.

We have verified the findings from the previous AUET1 tunings that the Jimmy model is not able to fit N_{ch} and $\sum p_{\perp}$ observables at the same time. This most likely due to a missing mechanism like colour reconnection, whose implementation in Pythia and Herwig++ helps to solve this problem. Given these observed limitations, it is likely that the AUET2 tunings are the last tunings of Herwig/Jimmy within ATLAS and that future tuning activities will concentrate on the actively developed Herwig++.

Acknowledgements

We would also like to thank T. Sjöstrand and P. Skands for enlightening discussions, and the DESY NAF team for some last minute priority without which we could not have met the MC11 deadline.

References

[1] The ATLAS Collaboration, G. Aad et al., *Charged-particle multiplicities in pp interactions measured with the ATLAS detector at the LHC*, arXiv:1012.5104 [hep-ex].

[2] Atlas Collaboration, G. Aad et al., *Measurement of underlying event characteristics using charged particles in pp collisions at $\sqrt{s} = 900$GeV and 7 TeV with the ATLAS detector*, arXiv:1012.0791 [hep-ex].

[3] ATLAS Collaboration, G. Aad et al., *Measurements of underlying-event properties using neutral and charged particles in pp collisions at 900 GeV and 7 TeV with the ATLAS detector at the LHC*, arXiv:1103.1816 [hep-ex].

[4] Atlas Collaboration, G. Aad et al., *Measurement of inclusive jet and dijet cross sections in proton-proton collisions at 7 TeV centre-of-mass energy with the ATLAS detector*, Eur. Phys. J. **C71** (2011) 1512, arXiv:1009.5908 [hep-ex].

[5] C. ATLAS, *First tuning of HERWIG/JIMMY to ATLAS data*, Tech. Rep. ATL-PHYS-PUB-2010-014, CERN, Geneva, Oct, 2010. http://cdsweb.cern.ch/record/1303025.

[6] A. Buckley, *CEDAR: tools for event generator tuning*, PoS **ACAT2007** (2007) 050, arXiv:0708.2655 [hep-ph].

[7] A. Buckley et al., *Rivet user manual*, arXiv:1003.0694 [hep-ph].

[8] A. Buckley, H. Hoeth, H. Lacker, H. Schulz, and J. E. von Seggern, *Systematic event generator tuning for the LHC*, Eur.Phys.J. **C65** (2010) 331–357, arXiv:0907.2973 [hep-ph].

[9] T. Sjöstrand, S. Mrenna, and P. Skands, *PYTHIA 6.4 Physics and Manual*, JHEP **05** (2006) 026, arXiv:hep-ph/0603175.

[10] DELPHI Collaboration, P. Abreu et al., *Tuning and test of fragmentation models based on identified particles and precision event shape data*, Z. Phys. **C73** (1996) 11–60.

[11] The ATLAS Collaboration, *ATLAS Monte Carlo tunes for MC09*, ATLAS Note (2010) . http://cdsweb.cern.ch/record/1247375. ATL-PHYS-PUB-2010-002.

[12] A. Moraes, *Modeling the underlying event: generating predictions for the LHC*, . http://cdsweb.cern.ch/record/1168736/. ATLAS proceedings ATL-PHYS-PROC-2009-045.

[13] The CDF Collaboration, D. E. Acosta et al., *Study of jet shapes in inclusive jet production in $p\bar{p}$ collisions at $\sqrt{s} = 1.96$ TeV*, Phys.Rev. **D71** (2005) 112002, arXiv:hep-ex/0505013 [hep-ex].

[14] The ATLAS Collaboration, G. Aad et al., *Study of Jet Shapes in Inclusive Jet Production in pp Collisions at sqrt(s) = 7 TeV using the ATLAS Detector*, arXiv:1101.0070 [hep-ex]. * Temporary entry *.

[15] P. Z. Skands, *Tuning Monte Carlo Generators: The Perugia Tunes*, Phys. Rev. **D82** (2010) 074018, arXiv:1005.3457 [hep-ph].

[16] A. Sherstnev and R. Thorne, *Different PDF approximations useful for LO Monte Carlo generators*, arXiv:0807.2132 [hep-ph].

[17] A. Sherstnev and R. Thorne, *Parton Distributions for LO Generators*, Eur.Phys.J. **C55** (2008) 553–575, arXiv:0711.2473 [hep-ph].

[18] The OPAL Collaboration, K. Ackerstaff et al., *Measurements of flavour dependent fragmentation functions in Z0 → q anti-q events*, Eur. Phys. J. **C7** (1999) 369–381, arXiv:hep-ex/9807004.

[19] Particle Data Group Collaboration, C. Amsler et al., *Review of particle physics*, Phys. Lett. **B667** (2008) 1–1340.

[20] ALEPH Collaboration, R. Barate et al., *Studies of quantum chromodynamics with the ALEPH detector*, Phys. Rept. **294** (1998) 1–165.

[21] ALEPH Collaboration, A. Heister et al., *Studies of QCD at e+ e- centre-of-mass energies between 91-GeV and 209-GeV*, Eur. Phys. J. **C35** (2004) 457–486.

[22] G. Barker, E. Ben-Haim, M. Feindt, U. Kerzel, P. Roudeau, L. Ramler, and A. Savoy-Navarro, *A Study of the b-Quark Fragmentation Function with the DELPHI Detector at LEP I. oai:cds.cern.ch:994376*, Tech. Rep. DELPHI-2002-069-CONF-603. CERN-DELPHI-2002-069-CONF-603, CERN, Geneva, Jul, 2002. http://cdsweb.cern.ch/record/994376.

[23] JADE Collaboration, P. Pfeifenschneider et al., *QCD analyses and determinations of alpha(s) in e+ e- annihilation at energies between 35-GeV and 189-GeV*, Eur. Phys. J. **C17** (2000) 19–51, arXiv:hep-ex/0001055.

[24] S. Catani, B. Webber, and G. Marchesini, *QCD coherent branching and semiinclusive processes at large x*, 1991. Nucl.Phys. **B349** (1991) 635–654.

[25] *Pythia6 Update Notes*, http://www.hepforge.org/archive/pythia6/update_notes-6.4.25.txt.

[26] S. Zenz, *Measurement of Jet Cross Section and Fragmentation Using Tracks with the ATLAS Detector*, Tech. Rep. ATL-PHYS-PROC-2010-135, CERN, Geneva, Dec, 2010. http://cdsweb.cern.ch/record/1311502.

[27] The ATLAS Collaboration, G. Aad et al., *Measurement of Dijet Azimuthal Decorrelations in pp Collisions at* $\sqrt{s} = 7$ *TeV*, arXiv:1102.2696 [hep-ex]. * Temporary entry *.

[28] The ATLAS Collaboration, G. Aad et al., *Measurement of the production cross section for W-bosons in association with jets in pp collisions at sqrt(s) = 7 TeV with the ATLAS detector*, Phys.Lett.B (2010) , arXiv:1012.5382 [hep-ex].

[29] The CDF Collaboration, A. A. Affolder et al., *The transverse momentum and total cross section of* e^+e^- *pairs in the Z boson region from* $p\bar{p}$ *collisions at* $\sqrt{s} = 1.8$ *TeV*, Phys. Rev. Lett. **84** (2000) 845–850, arXiv:hep-ex/0001021.

[30] The DØ Collaboration, V. M. e. a. Abazov, *Measurement of dijet azimuthal decorrelations at central rapidities in* $p\bar{p}$ *collisions at* $\sqrt{s} = 1.96$ *TeV*, Phys. Rev. Lett. **94** (2005) 221801, arXiv:hep-ex/0409040.

[31] A. Buckley et al., *General-purpose event generators for LHC physics*, arXiv:1101.2599 [hep-ph].

[32] The CDF Collaboration, T. Aaltonen et al., *Measurement of Particle Production and Inclusive Differential Cross Sections in* $p\bar{p}$ *Collisions at* $\sqrt{s} = 1.96$ *TeV*, Phys. Rev. **D79** (2009) 112005, arXiv:0904.1098 [hep-ex].

[33] The CDF Collaboration, A. A. Affolder et al., *Charged jet evolution and the underlying event in* $p\bar{p}$ *collisions at 1.8 TeV*, Phys. Rev. **D65** (2002) 092002.

[34] The CDF Collaboration, D. E. Acosta et al., *The underlying event in hard interactions at the Tevatron $\bar{p}p$ collider*, Phys. Rev. **D70** (2004) 072002, arXiv:hep-ex/0404004.

[35] The CDF Collaboration, T. Aaltonen et al., *Studying the Underlying Event in Drell-Yan and High Transverse Momentum Jet Production at the Tevatron*, Phys. Rev. **D82** (2010) 034001, arXiv:1003.3146 [Unknown].

[36] Pumplin, J. and others, *New generation of parton distributions with uncertainties from global QCD analysis*, JHEP **07** (2002) 012, arXiv:hep-ph/0201195.

[37] A. D. Martin, W. J. Stirling, R. S. Thorne, and G. Watt, *Parton distributions for the LHC*, Eur. Phys. J. **C63** (2009) 189–285, arXiv:0901.0002 [hep-ph].

[38] H.-L. Lai et al., *Parton Distributions for Event Generators*, JHEP **04** (2010) 035, arXiv:0910.4183 [hep-ph].

[39] P. M. Nadolsky et al., *Implications of CTEQ global analysis for collider observables*, Phys. Rev. **D78** (2008) 013004, arXiv:0802.0007 [hep-ph].

[40] H.-L. Lai et al., *New parton distributions for collider physics*, Phys. Rev. **D82** (2010) 074024, arXiv:1007.2241 [hep-ph].

[41] H1 and ZEUS Collaboration, F. D. Aaron et al., *Combined Measurement and QCD Analysis of the Inclusive ep Scattering Cross Sections at HERA*, JHEP **01** (2010) 109, arXiv:0911.0884 [hep-ex].

[42] Aharrouche et al., *Double differential Z,W cross sections and their ratios in the electron channels*, Tech. Rep. ATL-COM-PHYS-2010-325, CERN, Geneva, Jun, 2010. http://cdsweb.cern.ch/record/1269075/.

[43] R. D. Ball et al., *Impact of Heavy Quark Masses on Parton Distributions and LHC Phenomenology*, arXiv:1101.1300 [hep-ph].